Daniele Sechi, Stefano Andreucci, Thomas Stevens, Vincenzo Pascucci, Age and significance of late Pleistocene Lithophyllum byssoides intertidal algal ridge, NW Sardinia, Italy, Sedimentary Geology, 2020, vol. 400

https://dx.doi.org/10.1016/j.sedgeo.2020.105618

Age and significance of late Pleistocene *Lithophyllum byssoides* intertidal algal ridge, NW Sardinia, Italy

Daniele Sechi[a], Stefano Andreucci[b], Thomas Stevens[c], Vincenzo Pascucci[ab]

[a]Department of Architecture, Design and Planning, Via Piandanna 4, 07100 Sassari, Italy

[b]Institute of Geology and Petroleum Technologies, Kazan Federal University (Kazan) RU

[c]Department of Chemical and Geological Sciences, University of Cagliari, Cittadella Universitaria (Blocco A), 20125 Monserrato, CA, Italy

[d]Department of Earth Sciences, University of Uppsala, Villavägen 16, 752 36 Uppsala, Sweden

Corresponding author: Vincenzo Pascucci (pascucci@uniss.it)

Abstract

Intertidal coralline red algal build-ups (*Lithophyllum byssoides* rims or ridges) are considered precise sea level markers and mostly used for Holocene sea level history. Several well-preserved patches of relict red algal ridges crop out along the north-west Sardinian coast (Mediterranean Sea, Italy) and have great potential in reconstructing the late Pleistocene sea level history of the western Mediterranean. The aim of this paper is to determine the sedimentary characteristics of the relict *Lithophyllum byssoides* build-ups cropping out along the Sardinian NW coast and to demonstrate how these can be used as past sea-level indicators. To establish a chronological framework for these deposits, luminescence dating (both quartz OSL and K-feldspar pIRIR$_{290}$) has been applied and allows for the *Lithophyllum byssoides* ridge formation to be assigned to Marine Isotopic Stage (MIS) 5e (132-112 ka). The studied relict ridges confirmed that MIS 5e sea-level was at least at 4 m above present, well matching the widely accepted last interglacial global sea-level curves. Hence, fossil *Lithophyllum byssoides* ridges can be used as stratigraphic and chronologic indicators of late Pleistocene sea-level. Moreover, the study has underlined that *Lithophyllum byssoides* may grow: (1) in sheltered places along high cliffy coasts forming bench-like structures, and (2) in high-energy environments on wave cut platforms around fallen blocks or potholes, first as isolated mounds and then merging to form reef-like structures.

Keywords: Algal ridge; OSL, pIRIR, last interglacial, MIS 5e, sea-level marker.

1. Introduction

Quaternary global sea-level fluctuations and past warm periods are widely studied in order to provide constraints on possible future climate and sea-level variations (Hearty et al., 2007; Cronin, 2012; Muhs et al., 2015; Lamothe, 2016; Rovere et al., 2016; Pascucci et al., 2018). Tropical coral reef successions play a crucial role in modelling Pleistocene Relative Sea-level (RSL) variations because they provide relatively good estimates of palaeo-water depth and can be precisely dated with Uranium/Thorium (U/Th) and radiocarbon (^{14}C) methods (e.g., Woodroffe and Webster, 2014; Camoin and Webster, 2015). Continuous coral elevation data have generated well-constrained sea-level reconstructions. However, coral reefs are geographically restricted to the intertropical zone. As such, there is the need to find alternative sea-level markers that are as precise as coral to establish RSL curves at latitudes where no coral markers are available. Coastal cave speleothems (Dorale et al., 2010; Mauz et al., 2015; Polyak et al., 2018), tidal notches (Ferranti et al., 2006; Antonioli et al., 2004, 2015; Andreucci et al., 2006) and beachrocks (Rovere et al., 2016) are the typical markers chosen to develop Quaternary relative sea-level curves in the mid-latitudes. However, these markers cannot always be precisely dated. One further set of possible highly sensitive sea-level markers are intertidal rhodophyte (red algae) *Lithophyllum byssoides* bioconstructions (Adey, 1986; Stiros and Pirazzoli, 2008; Morhange and Marriner, 2015; Vacchi et al 2016). Such structures, better known as *Trottoir* (*sensu* Pérès and Picard, 1964), occur extensively along the western Mediterranean coasts (Bosence, 1976, 1983a, b, 1985; Laborel, 1987; Bellan-Santini et al., 1994; Laborel and Laborel-Deguen, 1994; Laborel et al., 1994; Nalin et al., 2006; Basso et al., 2007; Faivre et al., 2013; Rovere et al., 2016). The lower elevational limit of such bioconstructions is defined as biological mean sea-level (i.e., the sharp transition between the midlittoral and the infralittoral zone) (Bosence, 1976). This corresponds to Mean Sea-level (MSL) with reasonable accuracy of ±0.2 m (or ±0.1 m; Adey, 1986; Shennan et al., 2015) for microtidal environments such as the Mediterranean Sea (Vacchi et al., 2016). However, use of such precise sea-level markers has been so far limited solely to the Holocene interval (Faivre et al., 2013; Woodroffe and Webster 2014, Camoin and Webster, 2015; Muhs et al., 2015). This is mostly due to the inherent difficulty in dating these deposits beyond the age limit of 50 ka for radiocarbon (Morhange and Marriner, 2015).

All along the NW coast of Sardinia, central Mediterranean Sea, several outcrops of encrusting carbonate algae interpreted as patches of relict Quaternary *Lithophyllum* ridges are present. They are tentatively ascribed to Marine Isotopic Stage (MIS) 5e (132-112 ka; Lisiecki and Raymo, 2005; Railsback et al., 2015) based on their stratigraphic position (Sechi et al., 2013, 2018) and preliminary luminescence ages (Pascucci et al., 2014).

Over the past 20 years, luminescence dating has proved to be a powerful technique in establishing absolute chronologies for siliciclastic-rich successions developed during the last ~200 ka in a variety of depositional environments (shallow and deep marine, coastal, desert, fluvial, alluvial, periglacial, etc.; Murray and Funder, 2003; Jacobs et al., 2008; Mauz et al., 2009; Andreucci et al., 2010a, 2012, 2014, 2017; Perez-Alberti et al., 2011; Rhodes, 2011; Pascucci et al., 2014; Stevens et al., 2014a, b; Zucca et al., 2014; Bateman, 2015; Carnicelli et al., 2015; Lamothe, 2016). Moreover, the development of new luminescence dating protocols (such as pIRIR – post Infra-Red Stimulated Luminescence) performed on K-feldspar mineral have extended the age range of the dating technique to potentially 300 ka (e.g., Thomsen et al., 2008; Buylaert et al., 2009, 2011, 2012; Thiel et al., 2011, 2012; Murray et al., 2014; Bateman, 2015; Carr et al., 2018; Stevens et al., 2018). Luminescence techniques have also provided good results in dating sedimentary bodies rich in carbonate clasts or cement (>70% of weight; Nathan and Mauz, 2008; Andreucci et al., 2009, 2010b; Fornós et al., 2009; Thiel et al., 2010; Stevens et al., 2014b). However, the luminescence dating of *Lithophyllum* ridges has only been tentatively explored by Pascucci et al. (2014).

The aim of this paper is to determine the depositional time of formation of these relict *Lithophyllum byssoides* bioconstructions cropping out along the Sardinian NW coast and to confirm how these carbonate deposits can be used as Pleistocene sea-level indicators. Absolute dating will be performed using the luminescence-dating approach. Combined with the paper aims, the sedimentary characteristics, palaeo-depth and growth forms of the studied late Quaternary algal ridges are defined.

2. Site setting

2.1. Coastal and climate setting

The Mediterranean Sea is microtidal with an average tidal range of 35 cm (Longhitano, 2010). Sardinia is the second largest island in the west Mediterranean Sea (Fig. 1A). The present-day NW coast of the island (from Alghero to Bosa, Fig. 1B, C) is characterized by high steep cliffs often bounding small embayments where sandy or gravelly pocket beaches occur. The base of cliffs may host tidal-notches and incipient intertidal *Lithophyllum byssoides* bioconstructions or large wave cut platforms on which rock falls are reworked and form incipient bouldery-cobbly beaches. Extensive seagrass meadows occur from -4 up to -35 m depth below mean sea-level. Pocket beaches are nourished by inland-derived coarse materials supplied by a complex system of ephemeral streams (mainly active in winter) and by storm waves that carry bioclasts from the seagrass meadows to the shore (compositional mixing, *sensu* Chiarella et al., 2017). Waves have an average height of about 3 m, to a maximum of 9 m during major storms. The island has a typical Mediterranean climate characterized by temperate rainy autumn and spring, a not very humid winter and a hot dry summer, with a sea-surface temperature between 12 and 25°C. The NW-W blowing wind (Mistral) dominates along the west coast and triggers a longshore current flowing in the same broad direction (Donda et al., 2008; APAT, 2010; Manca et al., 2013; Vicinanza et al., 2013).

2.2. Geological setting and Quaternary stratigraphy

Sardinia represents a segment of the south-European plate that was displaced with an anticlockwise rotation to the present position after the opening of the Liguro-Provençal basin during the Oligocene-early Miocene (Carmignani et al., 1995, 2016; Doglioni et al., 1999; Casula et al., 2001) (Fig. 1A). The island was affected by intense tectonic and volcanic activity that ended in the late Pleistocene (ca. 140 ka) and presently it is considered stable and affected only by a general subsidence of about 0.01-0.02 mm/y (Ferranti et al., 2006) or quasi stable (Casini et al., in press). The pre-Quaternary bedrock along the study areas shows great lithological variability with the tectonic juxtaposition of Mesozoic sedimentary rocks, mainly quartz-rich sandstones and conglomerates, and limestones/dolostones. Oligo-Miocene volcanics are widespread and Plio-Pleistocene basalts are also found in places (Fig. 1C).

The Quaternary stratigraphy is the result of sea-level fluctuations controlled by Milankovitch cycles (Lobo and Ridente, 2014). The Middle Pleistocene-Holocene sedimentary sequence of Sardinia has been recently subdivided by Pascucci et al. (2014, and references therein) into eight major unconformity bounded units (U0 to U7), mainly represented by repetition of shallow marine deposits (Transgressive - Highstand Systems Tracts), alluvial systems (Falling Stage Systems Tracts) and coastal dunes (Lowstand Systems Tracts) spanning in time from about 300 ka (Marine Isotopic Stage, MIS 8) to Present (MIS 1).

In the study area, the late Quaternary stratigraphy could be summarized as follows: the lowermost outcropping deposits are composed of high angle cross-laminated medium-grained sandstones interpreted as lowstand coastal dunes (Unit 2 - U2) and attributed to MIS 6 (190-133 ka). These are followed by 1-2 m thick coarse grained conglomerates normally overlain by an up to 1 m-thick highly fossiliferous red algal (mostly *Lithophyllum* spp) bindstone associated with serpulide and barnacle communities in life position. Conglomerates are interpreted as transgressive lags (*sensu* Massari and Parea, 1988) and the fossiliferous bindstone as relict algal ridge (*sensu* Mediterranean *Lithophyllum byssoides* trottoir) deposited during transgressive and the following early highstand system tracts. Based on stratigraphic correlation and limited luminescence dating, the conglomerates and algal ridge have been assigned to MIS 5e (132-112 ka) and therefore to the lower part of Unit 3 (Unit 3a - U3a) (Pascucci et al., 2014; Sechi et al., 2018).

The upper part of Unit 3 (Unit 3b – U3b) is generally represented by well-developed low angle foresets of medium to coarse grained sandstone layers (or by mixed sandstones and conglomerates layers), interpreted as prograding and downstepping pocket beach systems developed during the late highstand system tract. This upper unit has been assigned to MIS 5c stage (~100 ka) based on stratigraphic position and luminescence dating (Andreucci et al., 2010a; Sechi et al., 2013; Pascucci et al., 2014).

An erosive unconformity associated with a subaerial exposure interpreted as equivalent of an incised valley normally marks the beginning of the following falling stage. Red to brownish massive silty deposits interpreted as colluvia and incipient palaeosols, locally covering the erosive surface, are considered equivalent to an incised valley fill. They are assigned to MIS 4 (Unit 4 - U4, 75-65 ka) age (Pascucci et al., 2014; 2019). The following lowstand deposits are represented by high-angle trough-cross bedded medium to coarse-grained sandstones. They are interpreted as coastal aeolian dunes (Unit 5-U5) developed during the last glacial period when sea-level was up to 120 m lower than present (ca. 65 to 12 ka, MIS 3-2).

Here, five locations have been selected for analysis because relict *Lithophyllum* ridges are well exposed (Fig. 2):

(1) El Trò bay is a sand and gravel cliff-bounded pocket beach that is open westward and apparently protected by the strongest storms. The cliffs are composed of Triassic limestones and late Quaternary sandstones (Figs. 2A, 3).

(2) Punta Padre Bellu cove is a small cliff-bounded embayment facing west and protected by strong northerly wind and storms, characterized by dispersed fallen blocks on the shore platform. The cliffs are composed of Oligo-Miocene volcanic rocks and late Quaternary sandstones (Figs. 2B, 4).

(3) Burantino bay is characterized by two small sandy cliff-bounded pocket beaches opened westward and protected by SW strongest storms, fed by ephemeral streams. The cliffs are composed of Oligo-Miocene volcanic rocks and late Quaternary sandstones (Figs. 2C, 5A, 5B).

(4) S'Abba Drucche bay consists of a small embayment opened westward and bounded by two Oligo-Miocene volcanic promontories. The embayment is characterized by a wide wave cut platform on which several fallen boulders rest. The central part of the bay is dominated by a large strand plain and gravel beach fed by a local ephemeral stream (Figs. 2D, 5C, 5D).

(5) Porto Alabe coast is characterized by a high Oligo-Miocene volcanic rock cliff on which late Pleistocene aeolian sands were deposited. At the base of the sandstone cliffs, a large wave cut platform dominated by currently forming potholes occurs. This coast is one of the most exposed to northwesterly wind and storms (Figs. 2E, 6).

3. Methods

In order to determine the sedimentary characteristics, paleo-depth of formation and the depositional time of these relict *Lithophyllum* build-ups, a multidisciplinary approach was used. A detailed sedimentological and stratigraphical analysis of the sedimentary sequence cropping out in the selected locations was performed and 20 sections were logged. Palaeontological analysis on the algal bindstones was carried out. Twenty thin sections for microscope analysis were prepared for red algal identification and to recognize the siliciclastic component trapped in the algal crusts. At the study sites, selected algal ridges (five) and clastic sedimentary deposits cropping out below and above the ridges, were sampled (14 total samples), dated (or re-dated) using both quartz OSL and k-feldspar $pIRIR_{290}$ luminescence methods. Dating has allowed us to define the algal bindstone age (Table 1).

Lithophyllum byssoides bindstones were sampled for luminescence dating in the most favourable conditions, mostly depending on the thickness and visible presence of clastic grains. Because *Lithophyllum* byssoides is considered a precise sea-level marker (Rovere et al., 2016; Vacchi et al., 2016*),* to obtain information on the mean past sea-level elevation, the ridges were field measured following the scheme proposed by Shennan et al. (2015) and Rovere et al. (2016). Measures were acquired using both rulers and optical level with a millimetric vertical precision (error of about 10%; Pascucci et al., 2019). The elevation of sea level indicator (algal ridge) was measured considering as field elevation the highest outcropping part of the algal ridge. Field elevation was corrected with the tide elevation of the sampling time/day based on the data available for Porto Torres gauge (the north Sardinia gauge; https://mareografico.it).

For the calculation of relative index points, necessary to define the paleo sea-level, the Mean Sea-level (MSL), as the arithmetic mean of hourly heights observed, and the Highest Astronomical Tide (HAT) recorded in north Sardinia during year 2018 (source https://mareografico.it/) have been used.

Measuring has allowed us to create a suite of palaeo relative sea-level index points (Rovere et al., 2016; Vacchi et al., 2016) (Table 2).

Note that luminescence age uncertainties are normally at the one standard deviation level. Perhaps the main limiting factor in the application of luminescence dating to algal ridges and understanding sea-level histories is that, in comparison with other chronometric techniques, the errors is much higher, typically in the range 5–10% of the derived age (Bateman, 2015). Therefore, at the moment, luminescence ages are not so precise and cannot be used for very high resolution stratigraphy (millennia scale) and the derived ages (including error) are only indicative of interstadial/stadial substages, such as the entire MIS 5e.

3.1 Luminescence dating

3.1.1 Sample collection and preparation

Thirteen samples from the studied sections were collected for luminescence dating. Samples BUR (Cala Burantino, Alghero) from the algal ridge and SD2 from S'Abba Drucche (Bosa) fossil sandy beach system were collected in the same place as samples Bur* and SD2*, dated by Pascucci et al. (2014). These have been re-analysed to verify and confirm the K-feldspar derived $pIRIR_{290}$ chronology and to obtain reliable quartz OSL ages.

Samples of sandstone and algal bindstones for luminescence dating were collected as blocks (50x50x50 cm) and treated at the University of Sassari Luminescence Dating laboratory under subdued red light. For luminescence analysis, pure quartz and K-feldspar grains ranging in size from 90-250 µm were obtained after treating the collected blocks using routine laboratory protocols (Aitken, 1985; Stokes, 1992; Mauz et al., 2002). This wide grain size range was chosen because of low sand contents in the algal bindstones (Andreucci et al., 2010a; Pascucci et al., 2014). Luminescence samples, data, and ages are listed in Table 1.

3.1.2 Luminescence measurements

Luminescence analyses were performed at the Nordic Laboratory for Luminescence Dating (DTU Risø campus, Denmark), the Luminescence Dating Laboratory of the Department of Geography, Royal Holloway (UK) and the Luminescence Dating Laboratory of the Department of Architecture, Design and Planning, University of Sassari (Italy). Quartz and K-feldspar grains were mounted on stainless-steel discs as small size multi grain aliquots (~2 mm in diameter) (Duller, 2008). Measurements were made using automated Risø TL/OSL readers (DA-20 and DA-15; Bøtter-Jensen et al., 2010) with calibrated $^{90}Sr/^{90}Y$ beta sources (~0.15 Gy/s and ~0.08 Gy/s). A Photomultiplier (PMT) was employed to detect K-feldspar and quartz luminescence signals. Quartz grains were stimulated using an array of blue LEDs emitting at 470 nm and the luminescence signal detected through a UV filter window (Hoya U-340 glass filter; 280-380 nm). Infrared LEDs were used for stimulation of K-feldspar grains and the luminescence signal was detected in the blue-violet region through a Schott BG39/Corning 7-59 filter combination (350-415 nm).

IR depletion ratio tests (Duller, 2003) were conducted on each quartz sample to check for residual feldspar contamination. Almost all of the samples showed IR depletion ratios less ±10% of unity, with the exception of sample BUR that showed IR ratios ≥10% below unity. Quartz equivalent doses for most samples were measured using the Single Aliquot Regenerative (SAR) protocol (Murray and Wintle, 2000, 2003) (Table S1) but for BUR sample the Double-SAR protocol was applied. This procedure consists of an extra IRSL step at 125 °C for 100 s before the OSL stimulation to remove possible K-feldspar or other IR-responsive components (Banerjee et al., 2001) (Table S1). Furthermore, the OSL IR depletion ratio was monitored during standard equivalent dose (De) determination for all samples and these checks showed no failed aliquots (i.e., with IR ratios <0.9).

The OSL signal during SAR and Double-SAR protocols was stimulated at 125 °C for 60 s and the net signal was calculated using early background subtraction to maximize the contribution of the fast component (Cunningham and Wallinga, 2010). The first 0.8 s and the following 2 s of signal were chosen for signal and background integrations respectively. The SAR test dose was kept lower than the 30% of the natural value for all samples (Wintle and Murray, 2006).

K-feldspar grains were analysed using the post-Infrared Infrared stimulation at high temperature protocol (pIRIR$_{290}$) (Buylaert et al., 2009, 2011, 2012; Thiel et al., 2011) (Table S1). The net signal was calculated by the integration of the initial 2 s and the last 30 s (background) of the signal. The pIRIR$_{290}$ test dose was always kept around 50% of the natural value for all samples (Yi et al., 2016).

Standard luminescence tests for quartz and K-feldspar grains were undertaken on two samples (BUR and SD2) from Burantino and S'Abba Drucche sites considered to be representative of the two wider study areas of Alghero and Bosa (Fig. 2B, D; see supplementary material for experimental details). Representative samples BUR and SD2 respectively collected from the algal bindstone of Cala Burantino (BUR, Alghero, Fig. 3B) and from the S'Abba Drucche (Bosa) beach deposits pass all the luminescence tests (Pre-heath plateau; Dose recovery test, first IR plateau) and therefore were considered highly reliable for dating using this protocol.

Moreover the recycling (repetition of a SAR cycle) and recuperation (zero given dose SAR cycle) tests were monitored as internal checks during each aliquot analysis for all samples. Results of luminescence tests and the reproducibility of the protocols (SAR, Double-SAR and $pIRIR_{290}$) are discussed in the supplementary material.

Representative quartz SAR, Double-SAR OSL and $pIRIR_{290}$ dose response curves are shown in Figures S1 and S2 (see supplementary material). The dose response curves for both quartz and K-feldspar aliquots were fitted using a single saturating exponential function. At least 18 aliquots for each sample were measured. Aliquots were rejected based on standard criteria (recycling ratio exceeding 10% of unity; recuperation < 5%) and signal saturation levels (2xDo < De). The final De value of all samples was calculated using the weighted mean of all the accepted aliquots (see supplementary material for more details).

3.1.3 Dosimetry

The outer part of each sampled block (≥ 5 cm) was removed and used to determine the field and saturation water contents and the natural radioactivity (Dose rate; Dr). The radionuclide concentrations were measured on a laboratory high-resolution gamma spectrometer following the procedures described in Murray et al. (1987) and converted into dry gamma and beta dose rates based on conversion factors published by Guèrin et al. (2011). The studied sedimentary bodies have typically ≥80% of HCl dissolvable material. This is because red algae are encrusting organisms producing carbonate crusts, trapping shells and siliciclastic grains during their life and the new generation of algae directly stand over the dead ones resulting in a "rock-like" deposit already at the time of deposition (Bosence, 1985; Adley, 1986). The limited post-burial cementation of the pore spaces suggests minor dissolution/re-precipitation events. Thus, it is assumed that the present-day radionuclide concentrations have remained essentially unchanged throughout the site lifetime.

Measurements of present-day moisture content span from 3.8 to 9.5% of sample weight. The moisture, since the time of deposition, is assumed to be between present-day and saturated for each sample and an arbitrary uncertainty of 3% is taken into account. Final total dose rates (Dr) were corrected for moisture content and cosmic ray contribution (Prescott and Hutton, 1994). For K-feldspar the dose rate contribution from internal beta decay of ^{40}K was taken into account, assuming a K content of 12.5 ± 0.5% (Huntley and Baril, 1997). The concentration activity of the principal radionuclides and calculated dose rates are listed in Table S2.

4. Results

4.1 Algal ridge facies description and interpretation

The studied algal ridges rest directly over the bedrock or basal conglomerate lag and form bodies ranging from 20 cm up to 2 m in thickness (average 50 cm). The morphology of the deposits varies from isolated or fused mounds developed around boulders, to incipient forms (i.e., clast binding or micro atoll-like forms), to extensive tabular ridge-like structures (Figs. 3-6). In the field, the algal framework shows a highly fossiliferous character with dispersed marine shells and well-rounded pebble to boulder-sized clasts (Fig. 5B). All these clasts are amalgamated and binded by algae, to form a cloudy/lumpy mixed carbonate-siliciclastic structure (bindstone) (Fig. 7A). Occasionally, this structure could be more gravel dominated showing an alternation of conglomerate strata and poorly developed algal-rich layers (incipient forms) or small carbonate coatings around clasts. Algal bindstones vary in colour from white to yellow-brownish and show at their tops, in some cases, evidence of oxidation, small cavities, or karst features filled by sand (Fig. 7A). The external and internal growth form of red algae is in general very dense with laminar overgrowths of different layers due to the continued overlapping of new algal crusts on the dead ones (Fig. 7B). The associated marine fossil faunal assemblage is constituted by species strictly linked to a shallow littoral environment and comprises *Barnacles* spp., *Serpulides* spp., *Acanthocardia tuberculata*, *Patella ferruginea*, *Glycymeris glycemeris*, *Conus testudinarius* and *Thais haemastoma* (Fig. 7C, D). Algal crusts, at the contact with the bedrock (inner zone), follow an uneven surface, showing preferential horizontal expansion, whereas laminar overgrowth appears less orientated with a chaotic growing direction in the outer zone. Overgrowths are arranged in bundles and generally enclose the bioclastic and siliciclastic sediments (Fig. 7E, F). Analysis of the growth form, thallus and conceptacle characteristics (Fig. 7G), clearly indicate the dominant algal rocky builder is the *Lithophyllum byssoides* coralline red algae (Laborel, 1961, 1987; Pérès and Picard, 1964; Laborel et al., 1994; Laborel and Laborel-Deguen, 1994; Cossu and Gazale, 1997; Woelkerling et al., 1993; Flugel, 2010; Bracchi et al., 2014; Guiry and Guiry, 2015). Bioclasts are mostly dominated by fragments of red algae, shells, barnacles, serpulids, bryozoans, echinoid spines and sponge spicules. Algal nodules (rhodoids) ranging in size from few mm to 5 cm are also observed (Fig. 7A). The siliciclastic material is mainly characterized by well-rounded to sub-rounded quartz, alkali feldspars, rock fragments and opaque heavy minerals (extremely abundant in volcanic domains). This sandy component fills all the available spaces, forming lumpy structures, gradually bounded and enveloped by the new generation of laminar algal thalli (Fig. 7E-G).

4.2 *Stratigraphy and luminescence ages*

4.2.1 El Trò bay (Alghero)

At El Trò site, the late Pleistocene succession rests unconformably on Mesozoic carbonates and is characterized by sandy and/or conglomeratic deposits. The north side of the cove is dominated by trough- to low-angle cross-bedded sandstone alternated with poorly imbricated conglomeratic layer interpreted as upper shoreface deposits. The upper shoreface is dated at 127 ± 11 ka (OSL) and 131 ± 8 ka (pIRIR$_{290}$) and therefore assigned to MIS 5e (unit U3a of Pascucci et al., 2014; Log # of Fig. 3A). Unconformable well stratified, planar to low-angle sandstones grading to highly root-bioturbated sandy bodies rest on unit U3a and are interpreted as foreshore and backshore deposits of a prograding beach system. These deposits are dated to 94 ± 6 ka (OSL) and 100 ± 6 ka (pIRIR$_{290}$) and associated with the MIS 5c (unit U3b of Pascucci et al., 2014; Table 1).

The succession on the south side of the cove is characterized by poorly developed, slightly imbricated, seaward dipping, clast-supported cobble-pebble conglomerates with broken marine shells and coarse-medium grained sandstones (Figs. 2A, 3). The conglomerate is encrusted by a < 50 cm-thick *Lithophyllum byssoides* bindstone, which shows more gravelly character and poorer maturity when compared to the bindstones observed in other areas. It occurs along the bay at an elevation above present sea-level varying from +1.00 to +3.75 m (Fig. 3). This sedimentary body is interpreted as a gravel beach/transgressive lag associated with a poorly developed incipient *L. byssoides* algal ridge. The succession is capped by well-stratified, planar laminated medium to coarse-grained sandstone beds interpreted as the foreshore and backshore part of high energy mixed sand and gravel prograding beach system (Fig. 3).

The new samples for luminescence in the El Trò area are CV2 and CV4 (Fig. 3; Table 1). Sample CV2, collected in the algal ridge, yields an OSL age of 121 ± 13 ka, and a pIRIR$_{290}$ age of 127 ± 14 ka, in good agreement with each other (Table 1). Thus, the bioconstruction is assigned to MIS 5e (U3a) (Fig. 3). Sample CV4, collected in the uppermost sandstones, yields a quartz-OSL minimum age of 76 ka and a pIRIR$_{290}$ age of 103 ± 7 ka, and therefore is assigned to MIS 5c (U3b) (Fig. 3A).

4.2.2 Punta Padre Bellu cove (Alghero)

The algal ridge rests unconformable on the Oligocene volcanic bedrock and shows the maximum observed thickness (about 2.5 m) (Fig. 5) with a maximum elevation of 4 m above present sea-level. This ridge is overlain by a ca. 50 cm thick poorly laminated coarse-grained sandstone rich in granules and marine shell fragments, interpreted as the backshore part of a pocket sandy beach system (Fig. 4D, E). The sedimentary succession continues with a 2 m-thick palaeosol/colluvium capped by several metres of aeolian deposits, spanning from MIS 4 to MIS 3/2 (Unit 4) (Andreucci et al., 2010b).

Sample PPB1 has been collected on the algal ridge. Quartz grains, despite passing all the luminescence tests, yield a final OSL age (206 ± 18 ka) much older compared with the pIRIR $_{290}$ age (135 ± 8 ka; Table 1). However, the latter is considered more reliable because it is in good agreement with the general stratigraphical and chronological framework of the area, as well as with the adjacent ages presented here. Considering the highstand nature of the deposits and the derived ages, the algal ridge and is assigned to MIS 5e.

Sample PPB3, taken from the overlaying backshore deposits, yields OSL and pIRIR $_{290}$ ages of 116 ± 12 ka and 118 ± 11 ka, respectively. This deposit likely formed during the final phase of the MIS 5e highstand (U3a; Fig. 4B; Table 1).

4.2.3 Burantino Bay (Alghero)

At Burantino bay, the late Pleistocene succession rests on Oligocene volcanic rocks. It starts with well sorted, high angle laminated parallel or trough cross-bedded coarse grained sandstones OSL dated (quartz) to 150 ± 10 ka and is therefore assigned to MIS 6 (Unit 2, Fig. 5A). These sandstones are overlain by boulder and cobble conglomerate strata, on which up to 1 m-thick highly fossiliferous red algal bindstones lie (Fig. 5A, B). Red algae carbonates have been luminescence dated to 113 ± 7 ka (quartz) and 114 ± 8 ka (k-feldspar) and therefore assigned to MIS 5e (Pascucci et al., 2014). Carbonates are overlain by coarse-grained sandstones organized in dm-thick strata with sub-horizontal or low-angle cross stratification gently dipping seaward, indicating a prograding sandy beach system. The sandstones have been OSL dated to 97 ± 6 ka and 98 ± 8 ka, thus belonging to MIS 5c (Fig. 5A).

The new collected sample in the algal ridge (BUR) yields an OSL age of 140 ± 9 ka and pIRIR$_{290}$ age of 119 ± 6 ka (Fig. 5A). The OSL age differs from previous studies (Bur*), while pIRIR290 is in good agreement (Table 1; Fig. 5) and as such the algal ridge deposits are confirmed as MIS 5e.

4.2.4 S'Abba Drucche bay (Bosa)

At S'Abba Drucche bay, the late Pleistocene succession starts with massive basal conglomerates (50 cm thick) ranging in size from large pebbles to mega boulders reflecting the local volcanic bedrock. They are locally encrusted and overlapped by thick (up to 1 m) carbonate deposits made of vermetides, barnacles and red calcareous algae (*Lithophyllum* spp) with dispersed abundant pebbles, granules, medium to coarse sand and gastropods (*Conus* cfr. *testudinarius, Arca noae*), bivalves, and molluscs (*Patella ferruginea, Cardita senegalensis, Glycymeris glycymeris, Ostrea spp*). These carbonates have a mound shaped geometry, drape discontinuously the conglomerates, and occur at the maximum high above present sea-level of +3.5 m. They have a k-feldspar luminescence age of 125 ± 8 ka and are thus assigned to MIS 5e (Fig. 5C, D).

Coarse grained trough-cross bedded sandstones with dispersed pebbles and several marine shell fragments gradually passing upwards to medium to coarse grained, and seaward dipping sandstones up to 2.5 m thick lie on top of MIS 5e strata. The succession ends with 0.5 m thick medium to coarse grained, massive sandstones with root bioturbation increasing towards the top. Faint traces of trough-cross or high angle lamination are occasionally observable (Fig. 5C). This succession is interpreted as a well-developed high-energy prograding sand and gravel beach system where both the submerged (shoreface) and emerged (foreshore and backshore/dune) parts are preserved (Pascucci et al., 2009). The foreshore is luminescence dated to 96 ± 8 ka (k-feldspar) and is therefore assigned to MIS 5c (Fig. 5C).

A new sample was collected in the laminated sandstone SD2 and yields an OSL age of 93 ± 7 ka and $pIRIR_{290}$ age of 99 ± 6 ka, confirming the attribution of the unit to MIS 5c (Fig. 5D; Table 1).

4.2.5 Porto Alabe cove (Bosa)

The late Pleistocene stratigraphic succession starts with a high angle cross-bedded, very coarse grained, sandstone body interpreted as aeolian coastal dunes (Fig. 6A). The overlying marine succession is exposed only in a small cove. This consists of cobbly-pebbly coarse-grained sandstone rich in volcanic granules and fragments of shells (Fig. 6B). At the centre of the cove, the basal conglomerate gradually passes upward from a low angle cross-stratified seaward dipping coarse-grained sandstone to an incipient and mature algal bindstone (Fig. 6B, C). The transition between sandstones to carbonate is characterized by the alternation of algal crusts and cross-laminated sandstone layers rich in algal rhodoliths and volcanic granules. Often the algal bindstone directly rests on the dune system (Fig. 6A). The ridge is locally covered by a thin (50 cm-thick) coarse-grained sandstone layer characterized by small volcanic granules (Fig. 6A, B). The marine succession reaches a maximum elevation of 3.5 m above present sea-level and the maximum thickness of the algal ridge is 50 cm. Clastic deposits are interpreted as a prograding beach system and the topmost sandstone as backshore deposits. The marine succession is capped by 50 cm to 2 m of thick lens-like layers composed of brownish siltstone with scattered sub-angular granules and pebbles of volcanic origin, alternating with up to 6 m thick strongly bioturbated coarse-grained high angle cross-stratified sandstones (Fig. 6A, C). This most likely represents multiple colluvial deposits alternating with coastal dune deposits.

At Porto Alabe, all the quartz samples have luminescence signals close to or completely saturated. The chronological framework has therefore been established only based on the $pIRIR_{290}$ ages (Table 1; see supplementary material for more details).

The lowermost aeolian deposits (PA1) are dated at 176 ± 16 ka and assigned to MIS 6 (Fig. 6A, C).

The marine succession is dated from bottom to top as 139 ± 13 ka (beach system, PA2), 134 ± 13 ka (algal ridge, PA3) and 137 ± 10 ka (backshore, PA4). Thus, it corresponds to unit U3a and to highstand deposits of MIS 5e (Fig. 6).

Sample PA5 collected at the base of the upper dunes is dated to 91 ± 10 ka (Fig. 6A, C). The coastal dune/colluvial system is, therefore, assigned to the falling stage of late MIS 5 and most probably also to part of the following MIS 4 glacial phase.

5. Discussion

5.1 Lithophyllum byssoides *algal ridges as sea-level markers of MIS 5e*

The studied algal ridges, based on the luminescence dating performed here and initial results by Andreucci et al. (2010a), Pascucci et al. (2014) and Sechi et al. (2018), were developed during the last interglacial stage; that is, during the MIS 5e highstand (Fig. 8; Table 1). It is widely accepted that MIS 5e started at 132 ka, based on the midpoint of the benthic $\delta^{18}O$ record transition from MIS 6 to MIS 5e (Shackleton et al., 2002), and ended between 112 ± 1 ka based on the benthic $\delta^{18}O$ transition from about +4.1‰ to about +3.7‰ or pollen data (cooling event marked by a distinct change from thermophiles deciduous to conifer forests; Sánchez Goñi et al., 1999 ller and Sánchez-Goñi, 2007). The presence of silica grains (quartz and k-feldspar) trapped inside the studied *Lithopyllum byssoides* algal ridge have allowed this first systematic attempt to date this sea-level marker with luminescence techniques (Table 1). It should, however, be considered that the ages derived from the algal ridges, including the age error, encompass the interval 147-106 ka (134 ± 13 ka and 114 ± 8 ka); that is, they span from end of MIS 6 and to MIS 5d/c boundary (Fig. 8A; Table 1). Nevertheless, despite the large uncertainty on these ages, the studied relict *Lithophyllum byssoides* ridges yield a mean age of 126 ka and are consistent around this interval, confirming the MIS 5e attribution (Fig. 8B). Moreover, it should be noted that according to the proposed growth rate for this intertidal bindstone, ranging from 0.1 to 0.6 mm a^{-1} (Nelson, 2009; Faivre et al., 2013) the 2.2 m thick *L. byssoides* ridge of Punta Padre Bellu cove (Fig. 5) formed in an average time interval of 6 ka (minimum 4 ka, maximum 22 ka). Thus, we claim that these bioconstructions developed as incipient forms dominated by vertical aggradation during the very late part of the transgressive phase (132-128 ka, early MIS 5e) and evolved into mature ridges characterized by tabular progradation when sea-level reached its maximum highstand (early regressive stage); that is, during the “plateau” phase encompassing 124 to 116 ka (Polyak et al., 2018). Modern mature *L. byssoides* ridges of the microtidal Mediterranean Sea develop at Mean Sea-level (transition between the mid littoral and the infralittoral zone; Laborel and Laborel-Deguen, 1994; Morhange and Marriner, 2015; De Luca et al., 2018) with an extremely high vertical precision (± 20 cm; Vacchi et al., 2016). A similar growth position and vertical precision can be assumed for the studied relict algal ridges. Thus, these bindstones could be used to estimate the mean sea-level reached during MIS 5e highstand.

The palaeo sea-level elevation uncorrected for Glacial Isostatic Adjustment (GIA) of the studied MIS 5e algae ridges is here calculated following the equations (eq. 1 to 4) provided by Rovere et al. (2016). Data needed to solve these equations are: Field elevation (E), Index range (IR) and Reference water level (RWL). For *L. byssoides* ridges field elevation corresponds to the highest point of the algal bindstone with respect to the present Mean Sea-level observed in the field. Index range is the difference between the Highest Astronomical Tide (HAT) and the Mean sea-level

(MSL) (Vacchi et al., 2016) that is about 0.35 m in Sardinia (De Luca et al., 2018; Pascucci et al., 2019), and reference water level represents the mid-point of the Index range that is for the studied ridges about 0.15 m (IR/2). For example, the ridge of El Trò bay has a field elevation of about 3.75± 0.1 m asl, an Index range value of 0.3 m and a Reference water level of 0.15 m. Thus, the final paleo Relative Sea-level (pRSL) for El Trò ridge is 3.6 ± 0.2 m (E - RWL; 3.75 - 0.15) above the present sea-level uncorrected for GIA (Table 2; Fig. 8B). Given that most of the algal ridges show evident erosive surfaces at their tops, the calculated elevations seem to represent only the minimum relative sea-level elevation reached by the MIS 5e highstand in NW Sardinia. The results from all sites give a minimum pRSL of 2.9 ± 0.2 m, a maximum of 3.6 ± 0.2 m and an mean value of 3.3 ± 0.6 m asl uncorrected for GIA (Fig. 8B; Table 2). The obtained mean pRSL results from the algal ridges around Alghero and Bosa is in agreement with the GIA-uncorrected pRSL values of Majorcan (2.15 ± 0.75 m asl) and Sardinian coastal cave speleothems (4.3 ± 0.5 m asl; Tuccimei et al., 2012; Polyak et al., 2018) (Fig. 8B).

5.2 Algal ridge evolution and influencing factors

L. byssoides bioconstructions are concretions housing a high algal and invertebrate biodiversity that are considered a target for conservation efforts (Pezzolesi et al., 2017). This species were used, since the study of Pérès and Picard (1964), to define and map the infralittoral zone around the Meditteranean coasts and more recently to evaluate the rate of Holocene sea-level rise (e.g., Ballesteros et al. 2007; Faivre et al., 2013, 2019; Blanfuné et al., 2016). By contrast, few attempts have been made to determine the processes responsible for this algal ridge formation and evolution, or to determine whether different factors such as coastal lithology, sea-level fluctuations, coastal setting, and wave energy can activate and influence the algal ridge formation and its distinct adaptive forms. The last interglacial was an interval with warmer climate (or as warm) than today, with a low global ice volume, and high sea-level (about 5 m above the present sea-level) (Kukla et al., 2002). Today, in NW Sardinia, *L. byssoides* occurs only in very sheltered areas attached to the intertidal zone of steep cliffs where it forms tabular bench-like features (*trottoirs*) (Cossu et al., 1998; De Luca et al., 2018). Along the studied sites, instead, a great variety of different relic algal bindstone forms are identified in life position, showing features ranging from incipient rim to mature algal ridge (Figs. 9, 10). This implies that the varieties of scenarios where *L. byssoides* developed along the NW coasts of Sardinia during MIS 5e are no longer exist due, possibly in part, to the warmer conditions occurred during the last interglacial. This yields valuable information regarding the possible morphologically adaptive development of these forms related to the shore hydrodynamic setting and bedrock lithology.

Similar to coral reefs, the algal ridge "keep up" is mainly influenced by sea-level stability or gradual (very slowly) sea-level rise, whereas wave stress, sediment supply and bedrock lithology may cause the evolution of different adaptive forms (Fig. 9). However, under ideal stable sea-level conditions all these forms tend to converge and assume the same mature tabular aspect (Chemello, 2009).

If we consider a protected embayment such as Punta Padre Bello (Fig. 9A) the relationships between hydrodynamic (wave stress), coastal setting and algal ridge maturity indicate it formed on the more sheltered flank of the bay directly attached to volcanic bedrock. In this case, the northwestern headland almost completely reflects and diffracts the strongest NW waves and permits formation of a sheltered area of calm water and low sediment supply (low energy zone=LE, Fig. 9A). In such quiet environments, coralline algae can encrust and grow undisturbed even directly attached to the bedrock, and will tend to converge and assume a mature tabular bench-like aspect. By contrast, in the high-energy sector (HE of Fig. 9A), which directly faces storm waves, large wave cut platforms (15 m wide) formed and the "keep up" of algal ridges was completely inhibited. In such high-energy conditions, however, *L. byssoides* may benefit from blocks fallen from the retreating coast and forming boulder beaches at the base of cliff (Fig. 11A, step 1). These boulders cause wave-sheltered intertidal shady rocky environments where the wave stress is mitigated and incipient algal rims may find protected environments to develop as well. This scenario occurs at Burantino (Fig. 9B) and S'Abba Drucche (Fig. 9C) bays. Here, coralline algae encrusts the boulders at the tidal level and form rims around them (Fig. 10A, B). The later evolution of the rim towards a mature ridge is instead controlled by the sea-level position. Under slowly rising of the sea-level, algal rims grow on isolated blocks more vertically than laterally, following sea-level rise (Fig. 11A, step 2). When sea-level approaches a still-stand, coralline algae grows more laterally then vertically, forming mounds (Figs. 10C, 11A, step 2). During prolonged periods of sea-level stability, mounds may merge to form a unique tabular ridge (reef like structure) losing their original mound appearance (Fig. 11A, step 3 - mature algal ridge).

A third possible scenario is a wave-dominated high-energy environment where the wave cut platform is carved into a soft easily erodible substrate, with no boulders dispersed on the shore platform. This scenario is likely represented at Porto Alabe (Fig. 9D). The coastal setting here is mostly characterized by a steep cliff and a large high tide/wave cut platform formed in the soft, erodible, poorly consolidated sandy substrate. The characteristics of the bedrock and the highly erosive regime should prevent the formation of incipient encrusting algae forms, which would be easily eroded during major storms. However, even in this case coralline algae take advantage of the erosive potholes that may be carved on top of platform surface when clasts are carried on to it during major storms (Figs. 10D-F, 11B, step 1). Potholes act as traps for water and loose sediments during high tides or moderate storms. Coralline algae and other species take advantage of this sheltered humid microenvironment to survive, in particular during low tide (Fig. 10D, E). When sea-level rises, the platform surface is flooded and submerged and coralline algae may form incipient rims that primary fill and later spread out from the potholes forming an atoll-like feature (Figs. 10 F-H, 11B, step 2). When sea-level approaches its maximum and a still-stand occurs, the platform is completely submerged and algal rims could grow in thickness becoming thick enough to resist to the wave energy (Fig. 11B, step 3). During a long period of stability, isolated rims may merge to form a "reef-like" ridge that later might grow in thickness (Figs. 9D, 10I, 11 – mature algal ridge). During major energetic storms, part of the incipient algal crusts may be pulled out and accumulated as “rhodolithic-like” features on the shore together with clastic sediments (Fig. 10G). This extreme scenario is well represented at El Trò bay (Fig. 9E). The bay, as it is now, was narrow, elongated seaward toward SE, and protected from the NW coming storms by relatively low relief cliffs. However, it directly faced storms from the SW. The particular funnel shape of the bay acts as a trap for sediments, which accumulated on the shore forming a large high-energy mixed sand and gravel pocket beach. Incipient algal ridges begin to develop on the biggest clasts in the bay. However, during occasional SW major storms, the bay was highly stressed by the wave energy. During these strong events, incipient algal ridges were reworked, crushed and completely or partially destroyed. The derived clasts entered into the sediment budget available to nourish the beach. This may explain why in this area the algal ridges never reached a mature aspect and show the most gravelly character among all the areas examined (Figs. 3, 10E).

In sum, apart from sea-level position and stability, the combination of different factors such as waves stress (shore hydrodynamics), costal setting and lithology may lead to the formation and evolution of algal ridges from incipient to mature forms.

6. Conclusions

The study of MIS 5e relict *Lithophyllum byssoides* ridges on Sardinia have allowed testing the capability of both quartz OSL and K-feldspar $pIRIR_{290}$ luminescence methods in dating intertidal algal bioconstructions. A potential problem in dating relict marine deposits, such as the algal bioconstructions, is to establish the completeness of resetting of luminescence signal prior deposition. Samples suffering from signal partial bleaching may significantly overestimate the "true" burial age. Thus, it is mandatory to investigate whether samples were completely bleached prior deposition or not. We have explained and discussed in detail this point in the supplementary material. Conclusions are that luminescence dating on Sardinian relict *Lithophyllum byssoides* ridges and surrounding coastal sedimentary units shows that many of quartz OSL derived ages are likely unreliable, due to the weak signals or to quartz OSL signals in saturation. Nonetheless, the feldspar $pIRIR_{290}$ ages appear reliable and allowed development of a robust age dataset for the algal ridges and constrain their development within MIS5e (mean age 126 ka).

Lithophyllum byssoides algal ridge in NW Sardinia developed during the sea-level rise phases and successive still-stands (early regressive phase) that occurred during MIS 5e; that is, during the warmest phase of the last interglacial. This algal ridge developed in the shallow subtidal/intertidal zone and thus can be considered as an indicator of sea-level and a potential useful tool to calculate the palaeo shoreline elevation. In particular, the studied ridges in Sardinia clearly indicate that the mean position of pRSL uncorrected for GIA during MIS 5e was about 3.3 ± 0.6 m above present, in line with other regional estimates. It is worthy to note that, although the *Lithophyllum* byssoides algal ridge could potentially represents a very precise paleo sea level marker at cm scale, at the moment, with luminescence dating it is only possible to define if the studied ridge developed during the entire MIS5e or not. It is, therefore, impossible to precisely date at millennium scale when the sea level was at its maximum (or minimum) during the last interglacial.

The study has underlined that *L. byssoides* can develop directly on any kind of rocky substrate and eventually form a narrow *trottoir* in very protected areas. In high energy environments, the presence or absence of a basal boulder pavements above the shore platform are critical elements in controlling algal ridge development. Boulders may provide a wave-sheltered intertidal rocky environment where the wave stress is mitigated and incipient algal rims may find protected environments to develop. In this case, algal incipient growth forms developed as isolated mounds over the boulders and eventually merged, creating a tabular and continuous reef-like ridge. On easy erodible bedrock with no boulder pavements, the incipient *L. byssoides* algal crusts may benefit from the presence of potholes and develop isolated rims, eventually merging together to build up a tabular, laterally continuous and mature reef-like ridge.

Acknowledgments

We are grateful to Ahmed Elshazly for field assistance, to Jan-Pieter Buylaert for the important advice and data analysis support, and the authors wish to acknowledge the support of the Nordic Laboratory for Luminescence Dating (NLL) and the luminescence researcher team of DTU-Nutech. The revision of the Chief Editor Jasper Knight and anonymous reviewers strongly helped to improve the first version of the manuscript. We would like to thank Dr Simon Armitage and Mr Iñaki Valcarcel of Royal Holloway University of London for access and technical support. Financial support: to SA was provided by a grant from Regione Autonoma Sardegna: L.R. 7/2007, Bando 2012, Promozione della ricerca scientifica e dell'innovazione tecnologica in Sardegna, (resp. S. Andreucci) and to VP and DS by LR7/2007 RAS Ricerca di Base (Bando 2017) - Cambiamenti climatici e neotettonica – la Sardegna un continente semi-stabile (resp. V. Pascucci). Partial found to VP has been provided by the Russian Government Program of Competitive Growth of Kazan Federal University.

References

Adey, W.H., 1986. Coralline algae as indicators of sea-level. In: Van de Plassche O. (ed.), Sea-level Research: A Manual for the Collection and Evaluation of Data. Geo Books, Norwich, pp. 229-280.

Aitken, M.J., 1985. Thermoluminescence Dating. Academic Press, London, 267pp.

Andreucci, S., Pascucci, V., Clemmensen, L.B., 2006. Upper Pleistocene coastal deposits of West Sardinia: a record of sea-level and climate change. GeoActa 5, 79-96.

Andreucci, S., Clemmensen, Pascucci, V., 2009. Late Pleistocene coastal evolution of San Giovanni di Sinis (west Sardinia, Western Mediterranean). Sedimentary Geology 216, 104-116.

Andreucci, S., Clemmensen, L.B., Murray, A., Pascucci, V., 2010a. Middle to late Pleistocene coastal deposits of Alghero, northwest Sardinia (Italy): Chronology and evolution. Quaternary International 222, 3–16.

Andreucci, S., Clemmensen, L.B., Pascucci, V., 2010b. Transgressive dune formation along a cliffed coast at 75 ka in Sardinia, West Mediterranean: a record of sea-level fall and increased windiness. Terra Nova 22, 424-433.

Andreucci, S., Bateman, M.D., Zucca, C., Kapur, S., Akit, I., Dunajko, A., Pascucci, V., 2012. Evidence of Saharan dust in upper Pleistocene reworked palaeosols of North-west Sardinia, Italy: palaeoenvironmental implications. Sedimentology 59, 917–938.

Andreucci, S., Panzeri, L., Martini, I.P., Maspero, F., Martini, M., Pascucci, V., 2014. Evolution and architecture of a west Mediterranean upper Pleistocene to Holocene coastal apron-fan system. Sedimentology 61, 333–361.

Andreucci, S., Sechi, D., Buylaert, J.P, Sanna, L., Pascucci, V., 2017. Post-IR IRSL290 dating of K-rich feldspar sand grains in a wind-dominated system on Sardinia. Marine and Petroleum Geology 87, 91-98.

Antonioli, F., Bard, E., Potter, E., Silenzi, S., Improta, S., 2004. 215-ka History of sea-level oscillations from marine and continental layers in Argentarola Cave speleothems (Italy). Global and Planetary Change 43, 57–78.

Antonioli, F., Lo Presti, V., Rovere, A., Ferranti, L., Anzidei, M., Furlani, S., Mastronuzzi, G., Orrù, P.E., Scicchitano, G., Sannino, G., Spampinato, C.R., Pagliarulo, R., Deiana, G., de Sabatam, E., Sansòn, P., Vacchi, M., Vecchio, A., 2015. Tidal notches in Mediterranean Sea: a comprehensive analysis. Quaternary Science Reviews 119, 66-84.

APAT, 2010. Agenzia per la Protezione dell'Ambiente per i Servizi Tecnici. Rete Ondametrica Nazionale. https://mareografico.it/

Ballesteros, E., Torras, X., Pinedo, S., Garcia, M., Mangialajo, L., De Torres, M., 2007. A new methodology based on littoral community cartography dominated by macroalgae for the implementation of the European Framework Directive. Marine Pollution Bulletin 55, 172–80.

Banerjee, D., Murray, A.S., Bøtter-Jensen, L., Lang, A., 2001. Equivalent dose estimation using a single aliquot of polymineral fine grains. Radiation Measurements 33, 73–94.

Basso D., Nalin R., Massari F., 2007. Genesis and composition of the Pleistocene Coralligène de plateau of the Cutro Terrace (Calabria, southern Italy). Neues Jahrbuchfür Geologie und Paläontologie– Abhandlungen 244, 173–182.

Bateman M.D., 2015. The application of luminescence dating in sea-level studies. In: Shennan, I., Long, A.J., Horton, B.P. (Eds), Handbook of Sea-Level Research. John Wiley & Sons, Oxford, pp. 404-417.

Bellan-Santini, D., lacaze, J.C., Poizat, C., 1994. Les biocénoses marines et littorales de Méditerranée, synthèse, menaces et perspectives-246, uséum National d'Histoire Naturelle, Paris.

Blanfuné, A., Boudouresque, C.F., Thibaut, T., Verlaque. M., 2016. The sea-level rise and the collapse of a Mediterranean ecosystem, the *Lithophyllum byssoides* algal rim. In: The Thiébault, S., Moatti, J-P., (Eds). Mediterranean Region under climate change: A scientific update. IRD Éditions, Marseille, pp. 285-289.

Bosence, D.W.J., 1976. Ecological studies on two unattached coralline algae from Western Ireland. Palaeontology 19, 365-395.

Bosence, D.W.J., 1983a. The occurrence and ecology of recent rhodoliths: a review. In: Peryt, T.M. (Ed.), Coated Grains. Springer, Berlin, pp. 225-242.

Bosence, D.W.J., 1983b. Coralline algal reef frameworks. Journal of the Geological Society, London 140, 365-376.

Bosence, D.W.J., 1985. The Coralligène of the Mediterranean – a recent analogue for Tertiary coralline algal limestones. In: Toomey, D.F., Nitecki, M.H. (Eds.), Palaeoalgology, contemporary research and applications. Springer, Berlin, pp. 212-225.

Bøtter-Jensen, L., Thomsen, K.J., Jain, M., 2010. Review of optically stimulated luminescence (OSL) instrumental developments for retrospective dosimetry. Radiation Measurements 45, 253-257.

Bracchi, V.A., Nalin, R., Basso, D., 2014. Paleoecology and dynamics of coralline dominated facies during a Pleistocene transgressive-regressive cycle (Capo Colonna marine terrace, Southern Italy). Palaeogeography, Palaeoclimatology, Palaeoecology 414, 296-309.

Buylaert, J.P., Murray, A.S., Thomsen, K.J., Jain, M., 2009. Testing the potential of an elevated temperature IRSL signal from K-feldspar. Radiation Measurements 44, 560– 565.

Buylaert, J.P., Thiel, C., Murray, A.S., Vandenberghe, D.A.G., Yi, S.W., Lu, H.Y., 2011. IRSL and post-IR IRSL residual doses recorded in modern dust samples from the Chinese Loess Plateau. Geochronometria 38, 432-440.

Buylaert, J.P., Jain, M., Murray, A.S., Thomsen, K.J., Thiel, C., Sohbati, R., 2012. A robust feldspar luminescence dating method for Middle and Late Pleistocene sediments. Boreas 41, 435-451.

Camoin, G.F., Webster, J.M., 2015. Coral reef response to Quaternary sea-level and environmental changes: State of the science. Sedimentology 62, 401–428.

Carmignani, L., Decandia, F.A., Disperati, L., Fantozzi, P.L., Lazzarotto, A., Liotta, D., Oggiano, G., 1995. Relationship between the tertiary structural evolution of the Sardinia-Corsica-Provençal Domain and Northern Apennines. Terra Nova 7, 128-137.

Carmignani, L., Oggiano, G., Funedda, A., Conti, P., Pasci, S., 2016. The geological map of Sardinia (Italy) at 1:250,000 scale. Journal of Maps 12, 826-835.

Carnicelli, S., Benvenuti, M., Andreucci, S., Ciampalini, R., 2015. Late Pleistocene relic Ultisols and Alfisols in an alluvial fan complex in coastal Tuscany. Quaternary International 376, 163-172.

Carr, A.S., Haya, A.S., Powella, D.M., Livingstone, I., 2018. Testing post-IR IRSL luminescence dating methods in the southwest Mojave Desert, California, USA. Quaternary Geochronology 49, 85–91.

Casula, G., Cherchi, A., Montadert, L., Murru, M., Sarria, E., 2001. The Cenozoic grabens system of Sardinia: geodynamic evolution from new seismic and field data. Marine and Petroleum Geology 18, 863-888.

Chemello, R., 2009. Le biocostruzioni marine in Mediterraneo. Lo stato delle conoscenze sui reef a vermeti. Biologia Marina Mediterranea 16, 2-18.

Chiarella, D., Longhitano, S.G., Tropeano, M., 2017. Types of mixing and heterogeneities in siliciclastic-carbonate sediments. Marine and Petroleum Geology 88, 617-627.

Cossu, A.V.L., Gazale, V., 1997. Osservazioni ecologiche sulla distribuzione di Lithophyllum lichenoides Philippi (Corallinales, Rhodophyta) nelle isole della Sardegna settentrionale. Bollettino della Società sarda di Scienze Naturali 31, 101-119.

Cronin, T.M., 2012. Rapid sea-level rise. Quaternary Science Reviews 56, 11-30.

Cunningham, A.C., Wallinga, J., 2010. Selection of integration time intervals for quartz OSL decay curves. Quaternary Geochronology 5, 657-666.

De Luca, M., Pascucci, V., Gazale, V., Ruiu, A., Massetti, L., Cossu, A., 2018. Marine benthic forms of the Marine Protected Area Capo Caccia-Isola Piana (Sardinia, Italy). Journal of Maps 14, 421-427.

Doglioni, C., Gueguen, E., Harabaglia, P., Mongelli, F., 1999. On the origin of W-directed subduction zones and applications to the western Mediterranean. In: Groppelli, G., Viereck-Goette, L. (Eds), Stratigraphy and Geology of Volcanic Areas. Geological Society of London, Special Publication 156, pp. 541–561.

Donda, F., Gordini, E., Rebesco, M., Pascucci, V., Fontolan, G., Lazzari, P., Mosetti, R., 2008. Shallow water sea-floor morphologies around Asinara Island (NW Sardinia, Italy). Continental Shelf Research 28, 2550–2564.

Dorale, J.A., Onac, B.P., Fornós, J.J., Ginés, J., Ginés, A., Tuccimei, P., Peate, D.W., 2010. Sea-level 81,000 years ago in Mallorca. Science 327, 860-863.

Duller, G.A.T., 2003. Distinguishing quartz and feldspar in single grain luminescence measurements. Radiation Measurements 37, 161-165.

Duller, G.A.T., 2008. Single-grain optical dating of Quaternary sediments: why aliquot size matters in luminescence dating. Boreas 37, 589-612.

Faivre, S., Petricioli, T.B., Horvatinčić, N., Sironić, A., 2013. Distinct phases of relative sea-level changes in the central Adriatic during the last 1500 years — influence of climatic variations? Palaeogeography, Palaeoclimatology, Palaeoecology 369, 163–174.

Faivre, S., Bakran-Petricioli, T., Barešić, J., Horvatić, D., acario, K., 2019. Relative sea-level change and climate change in the Northeastern Adriatic during the last 1.5 ka (Istria, Croatia). Quaternary Science Reviews, 222, 1-18.

Ferranti, L., Antonioli, F., Mauz, B., Amorosi, A., Dai Pra, G., Mastronuzzi, G., Monaco, C., Orrù, P., Pappalardo, M., Radtke, U., Renda, P., Romano, P., Sansò, P., Verrubbi, V., 2006. Markers of the last interglacial sea-level high stand along the coast of Italy: tectonic implications. Quaternary International 146, 30–54.

Flugel E. 2010. Microfacies of Carbonate rocks, Analysis, Interpretation and Application. Springer-Verlag, Berlin Heidelberg, 984 pp.

Fornós, J., Clemmensen, L.B., Gomez-Pujol, L., Murray, A.S., 2009. Late Pleistocene carbonate aeolianite deposits on Mallorca, western Mediterranean: a luminescence chronology. Quaternary Science Reviews 28, 2697-2709.

Guèrin, G., Mercier, N., Adamiec, C., 2011. Dose-rate conversion factors: update. Ancient TL 29, 5-8.

Guiry, M.D., Guiry, G.M., 2015. Algae Base. World-wide electronic publication, National University of Ireland, Galway. http://www.algaebase.org (accessed on 21 October 2015).

Hearty, P.J., Hollin, J.T., Neumann, A.C., O'Leary, M.J., McCulloch, M., 2007. Global sea-level fluctuations during the Last Interglaciation (MIS 5e). Quaternary Science Reviews 26, 2090-2112.

Huntley, D.J., Baril, M.R., 1997. The K content of the K-feldspars being measured in optical dating or in thermoluminescence dating. Ancient TL 15, 11–13.

Jacobs, Z., 2008. Luminescence chronologies for coastal and marine sediments. Boreas 37, 508-535.

Kukla, G.J., Bender, M.L., de Beaulieu, J-L., Bond, G.,Broecker, W.S., Cleveringa, P., Gavin, J.E., Herbert, T.D., Imbrie, J., Jouzel, J., Keigwin, L.D., Knudsen, K-L., McManus, J.F., Merkt, J., Muhs, D.R., Muller, H., Poore, R.Z., Porter, S.C., Seret, G., Shackleton, N.J., Turner, C., Tzedakis, P.C., Winograd, I.J., 2002. Last Interglacial Climates. Quaternary Research 58, 2-13.

Laborel, J., 1961. Le concrétionnement algal "coralligène" et son importance geomorphologique en Méditerranée. Recueil des traveaux de la Station marine. Endoume 23, 37-60.

Laborel, J., 1987. Marine biogenic constructions in the Mediterranean, A review. Scientific Reports of the Port-Cros National Park 13, 97-126.

Laborel, J., Laborel-Deguen, F., 1994. Biological indicators of relative sea-level variation and of co-seismic displacements in the Mediterranean area. Journal of Coastal Research 10, 395–415.

Laborel, J., Morhange, C., Lafont, R., Le Campion, J., Laborel-Deguen, F., Sartoretto, S., 1994. Biological evidence of sea-level rise during the last 4500 years on the rocky coasts of continental southwestern France and Corsica. Marine Geology 120, 203–223.

Lamothe, M., 2016. Luminescence dating of interglacial coastal depositional systems: Recent developments and future avenues of research. Quaternary Science Reviews 146, 1-27.

Lisiecki L.E., Raymo M.E., 2005. A Pliocene-Pleistocene stack of 57 globally distributed benthic $\delta^{18}O$ records. Paleoceanography 20, 1003, 1-17.

Lobo, J.F., Ridente, D., 2014. Stratigraphic architecture and spatio-temporal variability of high-frequency (Milankovitch) depositional cycles on modern continental margins: An overview. Marine Geology 352, 215-247.

Longhitano, S., 2010. The record of tidal cycles in mixed silici–bioclastic deposits: examples from small Plio–Pleistocene peripheral basins of the microtidal Central Mediterranean Sea. Sedimentology 58, 691-719.

Manca, E., Pascucci, V., De Luca, M., Cossu, A., Andreucci, S., 2013. Shoreline evolution related to coastal development of a managed beach in Alghero, Sardinia, Italy, Ocean & Coastal Management 85(A), 65–76.

Massari, F., Parea, G.C., 1988. Progradational gravel beach sequences in a moderate to high-energy, microtidal marine environment. Sedimentology 35, 881-913.

Mauz, B., Bode, T., Mainz, E., Blanchard, H., Hilger, W., Dikau, R., Zöller, L., 2002. The luminescence dating laboratory at the University of Bonn: equipment and procedures. Ancient TL 20, 53-61.

Mauz, B., Elmejdoub, N., Nathan, R., Jedoui, Y., 2009. Last interglacial coastal environments in the Mediterranean-Saharan transition zone. Palaeogeography, Palaeoclimatology, Palaeoecology 279, 137–146.

Mauz, B., Vacchi, M., Green, A., Hoffmann, G., Cooper, A., 2015. Beachrock: a tool for reconstructing relative sea-level in the far-field. Marine Geology 362, 1-16.

Morhange, C, Marriner, N., 2015. Archeological and biological relative sea-level indicators. In: Shennan, I., Long, A.J., Horton, B.P. (Eds), Handbook of Sea-Level Research. John Wiley & Sons, Oxford, pp. 146-156.

Muhs, D.R., Simmons, K.R., Meco, J., Porat, N., 2015. Uranium-series ages of fossil corals from allorca, Spain: The “Neotyrrhenian” high stand of the editerranean Sea revisited, Palaeogeography, Palaeoclimatology, Palaeoecology 438, 408-424.

ller, U. ., S nchez- o i, .F., 2007. egeta on dynamic in southern ermany during sotopic Stage 5 (130-70 kyr ago) In: Sirocko, F., Claussen, M., Litt, T., Sánchez-Goñi, M.F. (Eds), The Climate of Past Interglacials. Elsevier, Amsterdam, pp. 277-288.

Murray, A.S., Funder, S., 2003. Optically stimulated luminescence dating of a Danish Eemian coastal marine deposit: a test of accuracy. Quaternary Science Reviews 22, 1177-1183.

Murray, A.S., Wintle, A.G., 2000. Luminescence dating of quartz using an improved single-aliquot regenerative-dose protocol. Radiation Measurements 32, 57-73.

Murray, A.S., Wintle, A.G., 2003. The single aliquot regenerative dose protocol: potential for improvements in reliability. Radiation Measurements 37, 377-381.

Murray, A.S., Marten, R., Johnston, A., Martin, P., 1987. Analysis for naturally occurring radionuclides at environmental concentrations by gamma spectrometry. Journal of Radioanalytical and Nuclear Chemistry 115, 263–288.

urray, A.S, Schmidt, E.D, Stevens, T., Buylaert, J.P, arković, S.B, Tsukamoto, S., Frechen, ., 2014. Dating Middle Pleistocene loess from StariSlankamen (Vojvodina, Serbia). Limitations imposed by the saturation behaviour of an elevated IRSL signal. Catena 117, 34–42.

Nalin, R., Basso, D., Massari, F., 2006. Pleistocene coralline algal build-ups (coralligène de plateau) and associated bioclastic deposits in the sedimentary cover of Cutro marine terrace (Calabria, Southern Italy). In: Pedley, H.M., Carannante, G. (Eds). Geological Society, London, Special Publications, 255, pp. 11-22.

Nathan, R.P., Mauz, B., 2008. On the dose-rate estimate of carbonate-rich sediments for trapped charge dating. Radiation Measurements 43, 14-25.

Nelson, W.A., 2009. Calcified macroalgae–critical to coastal ecosystems and vulnerable to change: a review. Marine Freshwater Research 60, 787–801.

Pascucci, V., Martini, I.P., Endres, A., 2009. Facies and ground-penetrating-radar (GPR) characteristics of coarse-grained beach deposits of the uppermost Pleistocene glacial Lake Algonquin, Ontario Canada. Sedimentology 56, 529–545.

Pascucci, V., Sechi, D., Andreucci, S., 2014. Middle Pleistocene to Holocene coastal evolution of NW Sardinia (Mediterranean Sea, Italy). Quaternary International 328–329, 3–20.

Pascucci, V., De Falco, G., Del Vais, C., Melis, R.T., Sanna, I., Andreucci, S., 2018. Climate changes and human impact on the Mistras coastal barrier system (W Sardinia, Italy). Marine Geology, 395, 271-284.

Pascucci, V., Frulio, G., Andreucci, S., 2019. New Estimation of the Post Little Ice Age Relative Sea-level Rise. Geosciences 9, 348, doi:10.3390/geosciences9080348.

Pérès, J.M., Picard, J., 1964. Nouveau manuel de Bionomiebenthique de la MerMéditerranée. Recueil des traveaux de la Station marine. Endoume 31, 1-137.

Pérez-Alberti, A., Valcarcel Díaz, M., Martini, I.P., Pascucci, V., Andreucci, S., 2011. Upper pleistocene glacial valley-junction sediments at Pias, Trevinca Mountains, NW Spain. In: Martini, I.P., French, H.M., Pérez Alberti, A. (Eds), Ice-Marginal and Periglacial Processes and Sediments. Geological Society, London, Special Publications 354, pp. 93–110.

Pezzolesi, L., Falace, A., Kaleb, S., Hernandez-Kantun, J.J., Cerrano, C., Rindi, F., 2017. Genetic and morphological variation in an ecosystem engineer, *Lithophyllum byssoides* (corallinales, rhodophyta). Journal of Phycological Society of America 53, 146–160.

Polyak, V.J., Onac, B.P., Fornos, J.J., Hay, C., Asmerom, Y., Dorale, J.A., Gines, J., Tuccimei, P. Gines, A., 2018. A highly resolved record of relative sea-level in the western Mediterranean Sea during the last interglacial period. Nature Geoscience 11, 860-864.

Prescott, J.R., Hutton, J.T., 1994. Cosmic ray contributions to dose rates for luminescence and ESR dating: large depths and long-term variations. Radiation Measurements 23, 497–500.

Railsback, L.B., Gibbard, P.L., Head, M.J., Voarintsoa, N.R.G., Toucanne, S., 2015. An optimized scheme of lettered marine isotope substages for the last 1.0 million years, and the climatostratigraphic nature of isotope stages and substages. Quaternary Science Reviews 111, 94-106.

Rhodes, E.J., 2011. Optically stimulated luminescence dating of sediments over the past 200,000 years. Annual Review of Earth and Planetary Sciences 39, 461-488.

Rovere, A., Raymo,M.E., Vacchi, M., Lorscheid, T., Stocchi, P., Gómez-Pujol, L., Harris, D.L., Casella, E., O'Leary, M.J., Hearty, P.J., 2016. The analysis of Last Interglacial (MIS5e) relative sea-level indicators: Reconstructing sea-level in a warmer world. Earth-Science Reviews 159, 404-427.

Sánchez Goñi, M.F., Eynaud, F., Turon, J.L., Shackleton, N.J., 1999. High resolution palynological record off the Iberian margin: Direct land-sea correlation for the last interglacial complex. Earth and Planetary Science Letters 171, 123–137.

Sechi, D., Andreucci, S., Pascucci, V., 2013. High energy beaches system developing during MIS5c high sea-stand (100 ka), north-west Sardinia, Italy. Journal of Mediterranean Earth Sciences, Special Issue 5, 133-136.

Sechi, D., Andreucci, S., Pascucci, V., 2018. Intertidal Upper Pleistocene algal build-ups (Trottoir) of NW Sardinia (Italy): a tool for past sea-level reconstruction. Journal of Mediterranean Earth Sciences 10, 167-171.

Shackleton, N.J., Chapman, M., Sánchez-Goñi, M.F., Pailler, D., Lancelot, Y., 2002. The Classic Marine Isotope Substage 5e. Quaternary Research 58, 14–16.

Shennan, I., Long, A.J., Horton, B.P., 2015. Handbook of Sea-Level Research. John Wiley & Sons, Oxford, pp. 1-581.

Stevens, T., Paull, C., Ussler III, W., McGann, M., Buylaert, J.P., Lundsten, E., 2014a. The timing of sediment transport down Monterey Submarine Canyon, offshore California. Geological Society of America Bulletin 126, 103-121.

Stevens, T., Jestico, J.M., Evans, G., Kirkham, A., 2014b. Eustatic control of late Quaternary sea-level change in the Arabian/ Persian Gulf. Quaternary Research 82, 175–184.

Stevens, T., Buylaert, J. P., Thiel, C., Újvári, G., Yi, S., Murray, A. S., Lu, H., 2018. Ice-volume-forced erosion of the Chinese Loess Plateau global Quaternary stratotype site: Nature Communications 9, 983, doi: 10.1038/s41467-018-03329-2.

Stiros, S.C., Pirazzoli P.A., 2008. Direct determination of tidal levels for engineering applications based on biological observations. Coastal Engineering 55 , 459-467.

Stokes, S., 1992. Optical dating of young (modern) sediments using quartz: results from a selection of 26 depositional environments. Quaternary Science Reviews 11, 153–159.

Thiel, C., Coltorti, M., Tsukamoto, S., Frechen, M., 2010. Geochronology for some key sites along the coast of Sardinia (Italy). Quaternary International 222, 36–47.

Thiel, C., Buylaert, J.P., Murray, A.S., Terhorst, B., Hofer, I., Tsukamoto, S., Frechen, M., 2011. Luminescence dating of the Stratzing loess profile (Austria) - Testing the potential of an elevated temperature post-IR IRSL protocol. Quaternary International 234, 23-31.

Thiel, C., Buylaert, J.P., Murray, A.S., Elmejdoub, N., Jedoui, Y., 2012. A comparison of TT-OSL and post-IR IRSL dating of coastal deposits on Cap Bon peninsula, northeastern Tunisia. Quaternary Geochronology 10, 209-217.

Thomsen, K.J., Murray, A.S., Jain, M., Bøtter-Jensen, L., 2008. Laboratory fading rates of various luminescence signals from feldspar-rich sediment extracts. Radiation Measurements 43, 1474–1486.

Thomsen, K.J., Murray, A.S., Buylaert, J.P., Jain, M., Hansen, J.H., Aubry, T., 2016. Testing single-grain quartz OSL methods using sediment samples with independent age control from the Bordes-Fitterockshelter (Rochesd'Abilly site, Central France). Quaternary Geochronology 31, 77-96.

Tuccimei, P., Fornós, J., Ginés, A., Ginés, J., Gràcia, F., Mucedda, M., 2008. Sea-level change at Capo Caccia (NW Sardinia) and Mallorca (Balearic Islands) during oxygen isotope substage 5e, based on Th/U datings of phreatic overgrowths on speleothems. In: Pons, G.X., Vicens, D. (Eds.), Geomorfologia Litoral i Quaternari. Homenatge a Joan Cuerda Barcelo. Monografies de la Societat d'Historia Naturalde les Balears 14, pp. 121-136.

Tuccimei, P., Onac, B.P., Dorale, J.A., Ginés, J, Fornós, J.J, Ginés, A., Spada, G., Ruggieri, G., Mucedda, M., 2012. Decoding last interglacial sea-level variations in the western Mediterranean using speleothem encrustations from coastal caves in Mallorca and Sardinia: A field data-model comparison. Quaternary International 262, 56-64.

Vacchi, M., Marriner, N., Morhange, C., Spada, G., Fontana, A., Rovere, A., 2016. Multiproxy assessment of Holocene relative sea-level changes in the western Mediterranean: Sea-level variability and improvements in the definition of the isostatic signal. Earth-Science Reviews, 155, 172-197.

Vicinanza, D., Contestabile, P., Ferrante, V., 2013. Wave energy potential in the north-west of Sardinia (Italy). Renewable Energy 50, 506-521.

Waelbroeck, C., Labeyrie, L., Michel, E., Duplessy, J.C., McManus, J.F., Lambeck, K., Balbon, E., Labracherie, M., 2002. Sea-level and deep water temperature changes derived from benthic foraminifera isotopic records. Quaternary Science Reviews 21, 295–305.

Wintle, A.G., Murray, A.S., 2006. A review of quartz optically stimulated luminescence characteristics and their relevance in single- aliquot regeneration dating protocols. Radiation Measurements 41, 369–391.

Woelkerling, W.J., Irvine, L.M., Harvey, A.S., 1993. Growth-forms in non-geniculate coralline red algae (Corallinales, Rhodophyta). Australian Systematic Botany 6, 277-293.

Woodroffe, C.D., Webster, J.M., 2014. Coral reefs and sea-level change. Marine Geology 352, 248-267.

Yi, S., Buylaert, J.P., Murray, A.S., Lu, H., Thiel, C., Zeng, L., 2016. A detailed post-IR IRSL dating study of the Niuyangzigou loess site in northeastern China. Boreas 45, 644-657.

Zucca, C., Sechi, D., Andreucci, S., Shaddad, S.M., Deroma, M., Madrau, S., Previtali, F., Pascucci, V., Kapur, S., 2014. Pedogenic and palaeoclimatic evidence from an Eemiancalcrete in north-western Sardinia (Italy). European Journal of Soil Science 65, 420-435.

Table Captions

Table 1. Estimated equivalent dose (De) values and luminescence ages both for quartz (OSL) and K-feldspar samples (pIRIR$_{290}$). The samples are arranged in the table based on the geographic position of the studied sites, so the first entry at the top represents the northernmost study area. De values are calculated using the weighted mean $(De)^{W}$ of reliable aliquots $(n)^{R}$ of the total of analysed $(n)^{T}$, which overcome the applied recycling ratio rejection criteria and 2xDo < De criterion; (SAT) percentage of signal saturation (De/2D_0). (OD) overdispersion and (Skw) skewness values of De distribution. (Rd) estimated residual dose for piRIR$_{290}$. * = ages from Pascucci et al. (2014). De values were calculated using the weighted mean.

Table 2. Palaeo relative sea-level elevations uncorrected for GIA of the studied algal ridges. Reported field elevation corresponds to the highest elevation measured using a DGPS in the field; Index range is the difference between Highest Astronomical Tide and Mean Sea-level based on Vacchi et al. (2016) and pRSLis calculated following the equations of Rovere et al. (2015).

Figure captions

Fig. 1. (A) Location of Sardinia in the central western Mediterranean area. LPB = Liguro-Provençal basin. (B) Sardinia Island and location of the main cities. (C) Simplified geological map of North Sardinia (after Carmignani et al., 2016). The two main areas studied along the northwest coast of the island (Alghero and Bosa) and location of sub-areas studied. ET = EL Trò bay, PPB = Punta Padre Bellu cove, BUR = Burantino bay, SD for S'Abba Drucche bay and PA for Porto Alabe cove and position of the Cape (Cp) Caccia site described in Tuccimei et al. (2008).

Fig. 2. Morphological features of the studied areas. (A) El Trò bay bay, (B) Punta Padre Bellu cove, (C) Burantino bay, (D) S’Abba Drucche bay, and (E) Porto Alabe coast. Stars indicate the location of studied sections; geomorphologic details of the five areas are described in the text. Satellite images are form Google Earth, year 2017.

Fig. 3. (A) Satellite view of El Trò bay (ET) and location of stratigraphic logs (L1-L5). Legend describes the main sedimentary facies identified and their sedimentological interpretation. Filled black diamonds highlight luminescence ages performed by Pascucci et al. (2014) while the black squares mark the new sampling positions. All the ages are reported in ka. (B) Field view of an incipient algal ridge (MIS 5e-U3a) developed unconformably on a gravel lag and bedrock. The bedrock is represented by Triassic limestones. Seaward the algal ridge is covered by the gravel deposits interpreted as berm of the (MIS5c-U3b) beach system.

Fig. 4 (A) Satellite view and representative stratigraphic log of Pleistocene deposits cropping out at Punta Padre Bellu cove (PPB). Legend describes the main sedimentary facies identified and their sedimentological interpretation. All luminescence ages are reported in ka. (B) Field view of the algal ridge outcropping at PPB site and luminescence ages.

Fig. 5. Burantino (BUR) and S’Abba Drucche (SD) bays. Legend describes the main sedimentary facies identified and their sedimentological interpretation. Filled black diamonds highlight luminescence ages performed by Pascucci et al. (2014) whereas the black squares mark the new luminescence samples. All luminescence ages are reported in ka. (A) Satellite view of Burantino and location of stratigraphic logs (L1-3) reported below; (B) Detail of the algal ridge, sample location and luminescence (Q=OSL ad K= $pIRIR_{290}$) ages. ( ) Satellite view of S’Abba Drucche cove

and location of stratigraphic logs (L1-4) reported below. (D) Detail of the algal ridge, sample location and luminescence (Q=OSL and K= $pIRIR_{290}$) ages.

Fig. 6. (A) Porto Alabe coastal setting, position of the logs measured and stratigraphic sketches of the Pleistocene succession for both areas. Legend describes the main facies identified and their sedimentological interpretation. Full black squares mark the sampling positions, labels and estimated luminescence ages. All ages are reported in ka. (B) Detail of the algal-rim atoll-like feature encrusting the basal gravel lag, of the basal dunes (U2), and of the beach backshore coarse-grained sandstone (U3a). (C) Sea view of the Pleistocene succession cropping out at Porto Alabe. From the bottom of the sequence the basal dunes system of MIS 6 (U2) and the marine succession form a gravel/sandy beach grading to a well-developed algal ridge (U3a), unconformably capped by the dune system succession related to MIS 5c (U3b).

Fig. 7. (A) General sedimentary characteristics of the coralline algal framework in the field and in thin section: massive conglomerate made of coarse sand, well rounded pebbles, fragmented marine shells and algal encrusting layers forming carbonate clouds. (B) Detail of the well-developed leafy laminar growth form direction of the crustose red algal rocky builder *Lithophyllum byssoides*. (C) Community of barnacle spp. in life position partially filled by a secondary coarse sand and encrusted by patches of red algae. (D) Field detail of an encrusting colony of serpulides spp. (E) Thin section detail of the internal lumpy structures of algal encrusting thallus. Thallus of *Lithophyllum byssoides* (star marks) forms a cloud of carbonate material that surrounds and traps coarse-sand and marine bioclast components (hash mark). (F, G) Detail of *Lithophyllum byssoides* thallus and reproductive organ sporangial conceptacles (black arrows) and isolated conceptacle.

Noteworthy is the sharp sinuous contact between the algae thallus and the lumpy siliciclastic component rich in well-rounded heavy minerals.

Fig. 8. Relative sea-level elevations and luminescence ages of the studied *Lithophyllum byssoides* algal ridges. (A) Derived pIRIRSL *Lithophyllum byssoides* ages with 2σ error, plotted on the sea-level curve by Waelbroeck et al. (2002). (B) The new derived pRSL markers (white dots) from the studied area plotted on the GIA corrected sea-level curve by Ployak et al. (2018) and compared with the spelothems of NW Sardinia (Neptum Cave, Tuccimei et al., 2012 – white rectangle) and Maiorca (Polyak et al., 2018 – white triangle). Black dot is relative to the average age (error 5-10%) and elevation of the studied samples (see Table 2 for additional details).

Fig. 9. Influence of coastal setting and hydrodynamics on the evolution of the mature algal ridge. Downward are the different coastal settings studied in this work and related different characteristics of the algal ridge for each setting. (A) Punta Padre Bellu cove=PPB; (B) Burantino bay=BUR, ( ) S'Abba Drucche bay=SD, (D) Porto Alabe cove=PA, (E) El Trò bay=ET. Details are in chapter4.1.

Fig. 10. Detail of different algal ridge growth forms. (A) Incipient *Lithophyllum* algal ridge encrusting a boulder resting on a wave cut platform carved into sandstone (Burantino coves). (B) Incipient algal ridge formed on fallen boulders resting on the shore platform (Punta Padre Bellu cove). Hammer 40 cm long is used for scale. (C) Incipient algal mound forms developed on the sheltered part of two very close fallen boulders. Noteworthy is the incipient connection between the two mounds (S'Abba Drucche bay). (D) Currently forming pothole partially filled by siliciclastic material. Calcareous algae form rim on the edge of the hole (Porto Alabe). (E) Fossil pothole filled

by cemented pebbly conglomerate (Porto Alabe). (F) Wide relict pothole with thick pebbly conglomerates filling up the centre and incipient algal rim encrusting the edge of the hole (Porto Alabe). ( ) Detail of “rhodolite layer” at the base of algal ridge. n the inset square, detail of rhodolites between two sandy layers (Porto Alabe) is expanded. (H) Detail of two well-developed micro algal atoll-like features partially merged (Porto Alabe). (I) Well developed *Lithophyllum* ridge directly developed on the sandy beachface deposits (Porto Alabe).

Fig. 11. Stages of algal ridge development under a slowly rising and stable sea-level. (A) Algal ridge development along a rocky coast dominated by blocks fallen from retreating cliff and forming a boulder beach at the base of a cliff; step 1 - coralline algae encrust the boulders at the tidal level and form rims around them; step 2 - intermediate growth forms (mound-like) develop during slowly increasing rates of sea-level; step 3 - mature algal ridge characterizes the period of sea-level stability mainly coincident with the maximum level. (B) Evolution of algal ridge along a coast characterized by easy erodible substrate (sandstone) where potholes may form (Porto Alabe site for example); step 1 - erosive structures (potholes) dominate the surface of the wave-cut platform; step 2 - during increasing sea-level these structures are colonized by incipient forms of algal ridge; step 3 - during stable sea-level isolated algal ridges are able to spread out and (mature) cover the entire surface.

Highlights

- Sedimentary characteristics of the relict *Lithophyllum byssoides* build-ups cropping out along the Sardinian NW coast
- Use of *Lithophyllum byssoides* build-ups as past sea-level indicators.
- Dating of the relict *Lithophyllum byssoides* ridge using luminescence (both quartz OSL and K-feldspar $pIRIR_{290}$).
- Fossil *Lithophyllum byssoides* ridges can be used as stratigraphic and chronologic indicators of late Pleistocene sea level.

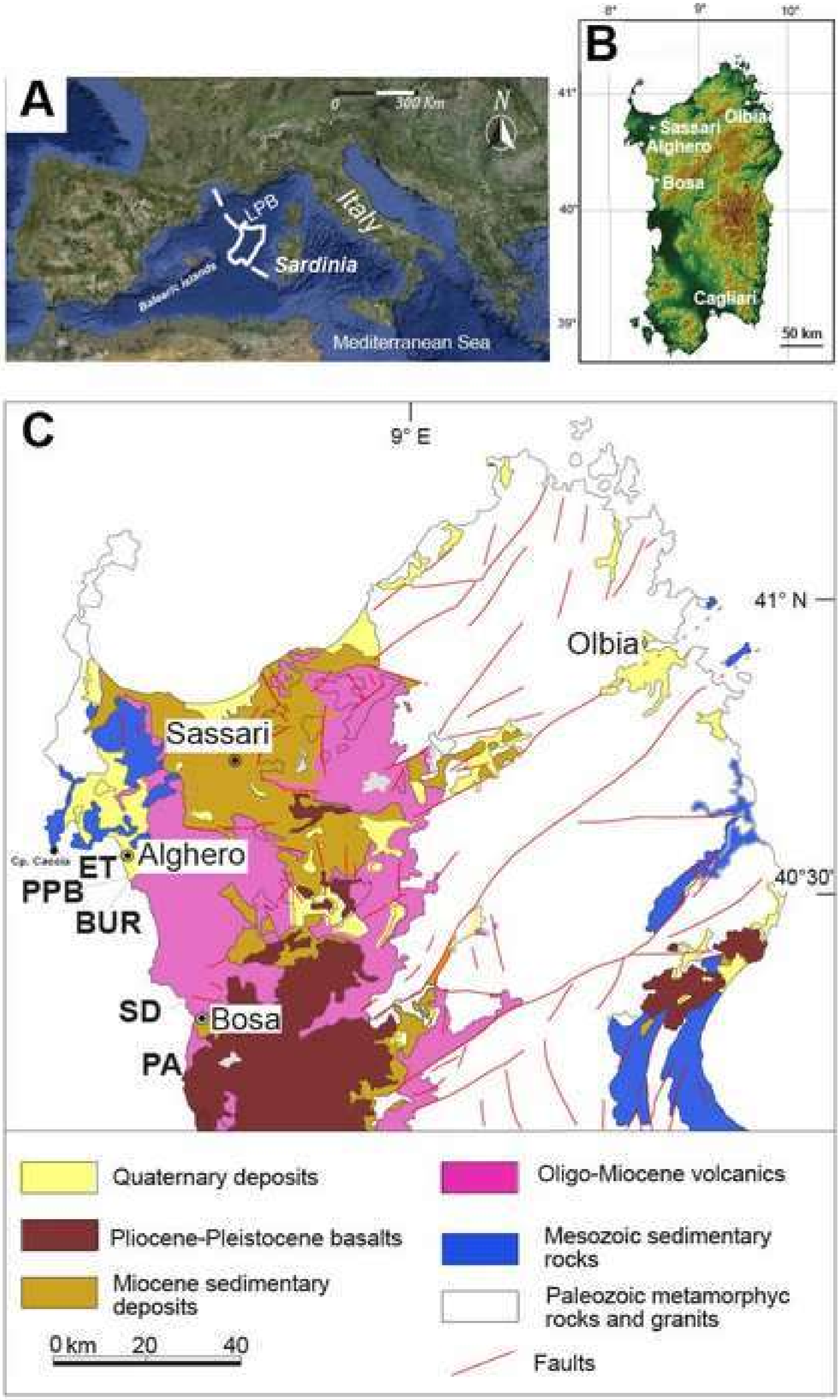
A
0
300 Km
N
LPB
Italy
Sardinia
Balearic Islands
Mediterranean Sea
B
8°
9°
10°
41°
40°
39°
Sassari
Olbia
Alghero
Bosa
Cagliari
50 km
C
9° E
41° N
40°30'
Olbia
Sassari
Alghero
Cp. Caccia
ET
PPB
BUR
SD
Bosa
PA
Quaternary deposits
Pliocene-Pleistocene basalts
Miocene sedimentary deposits
Oligo-Miocene volcanics
Mesozoic sedimentary rocks
Paleozoic metamorphyc rocks and granits
Faults
0 km
20
40

Figure

Click here to download high resolution image

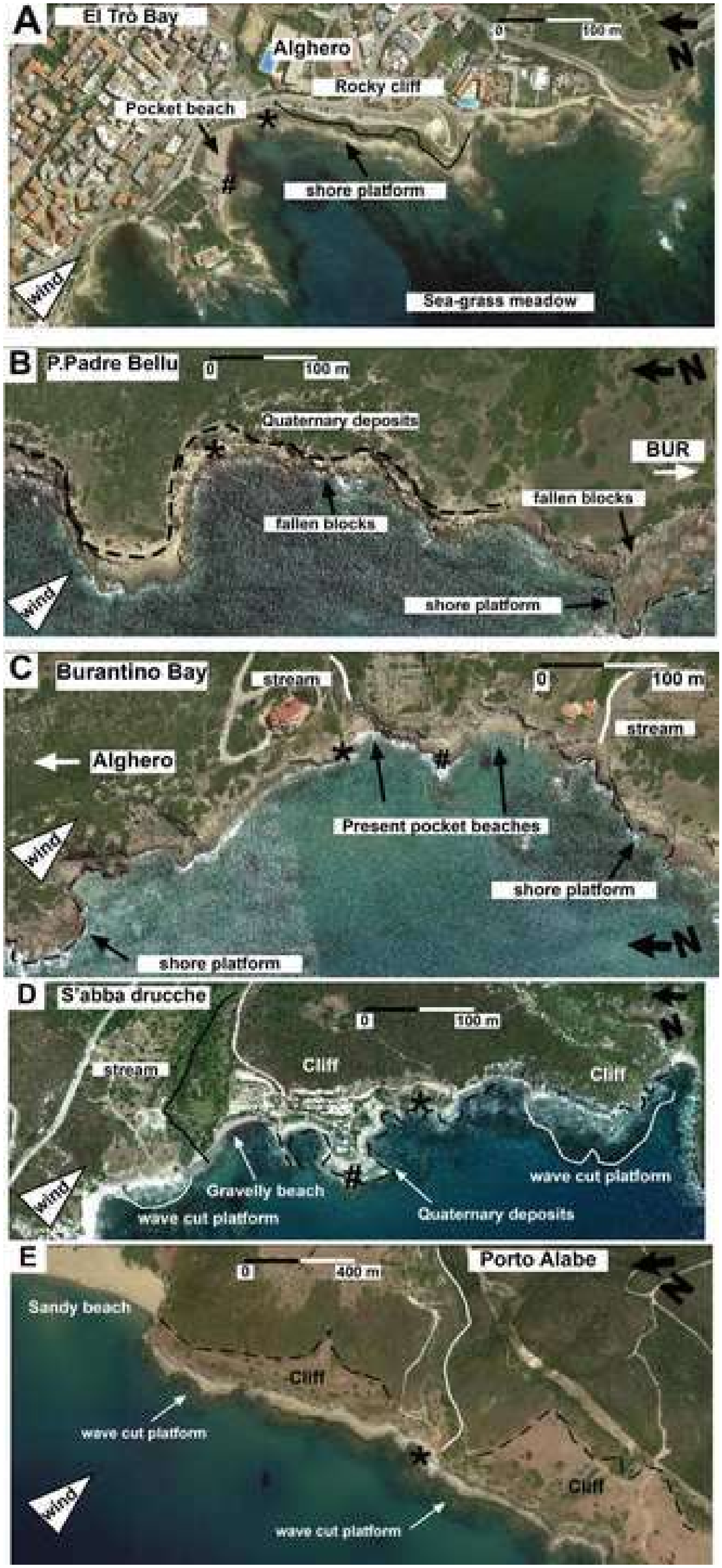

Figure
Click here to download high resolution image

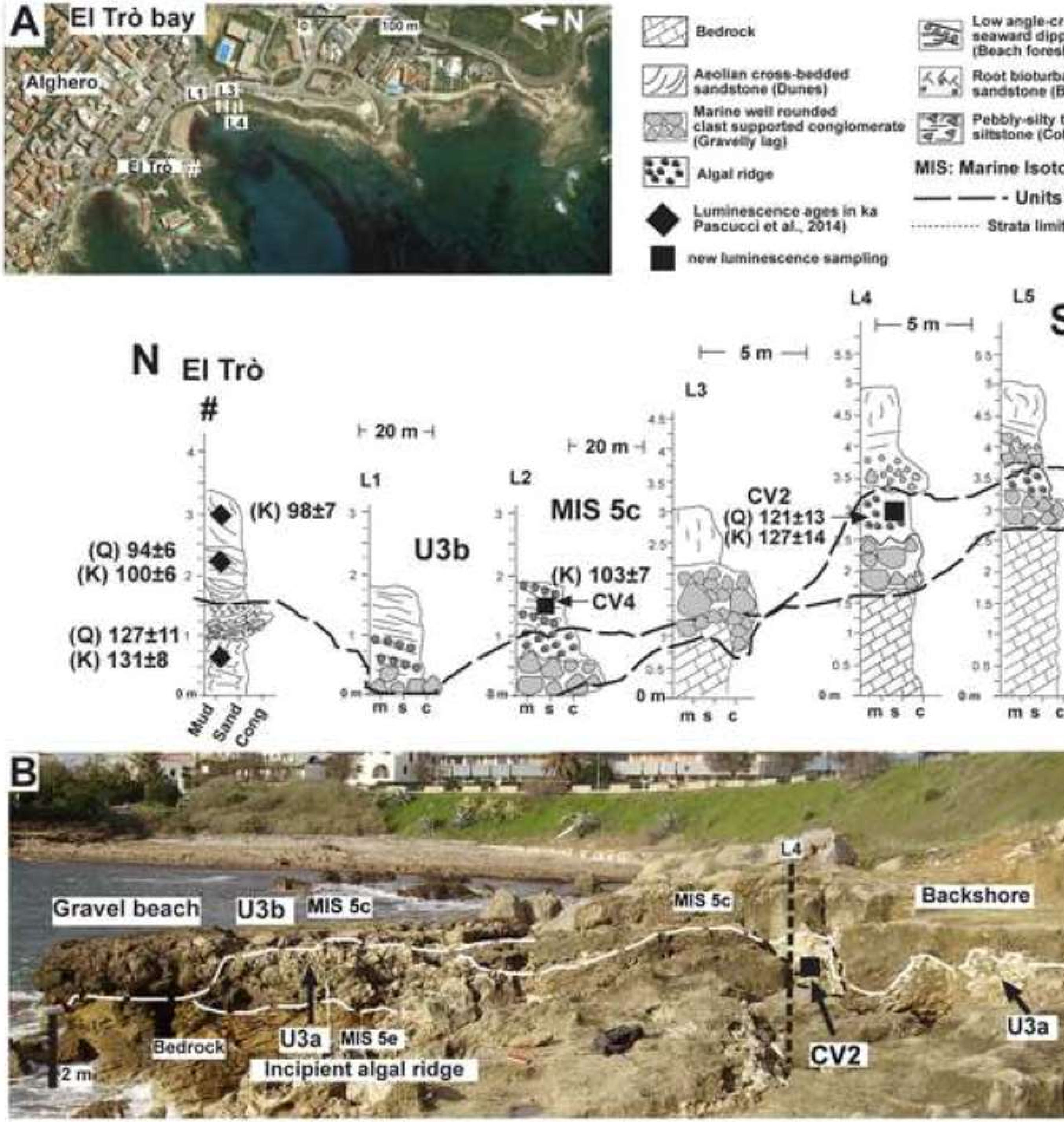

Figure
Click here to download high resolution image

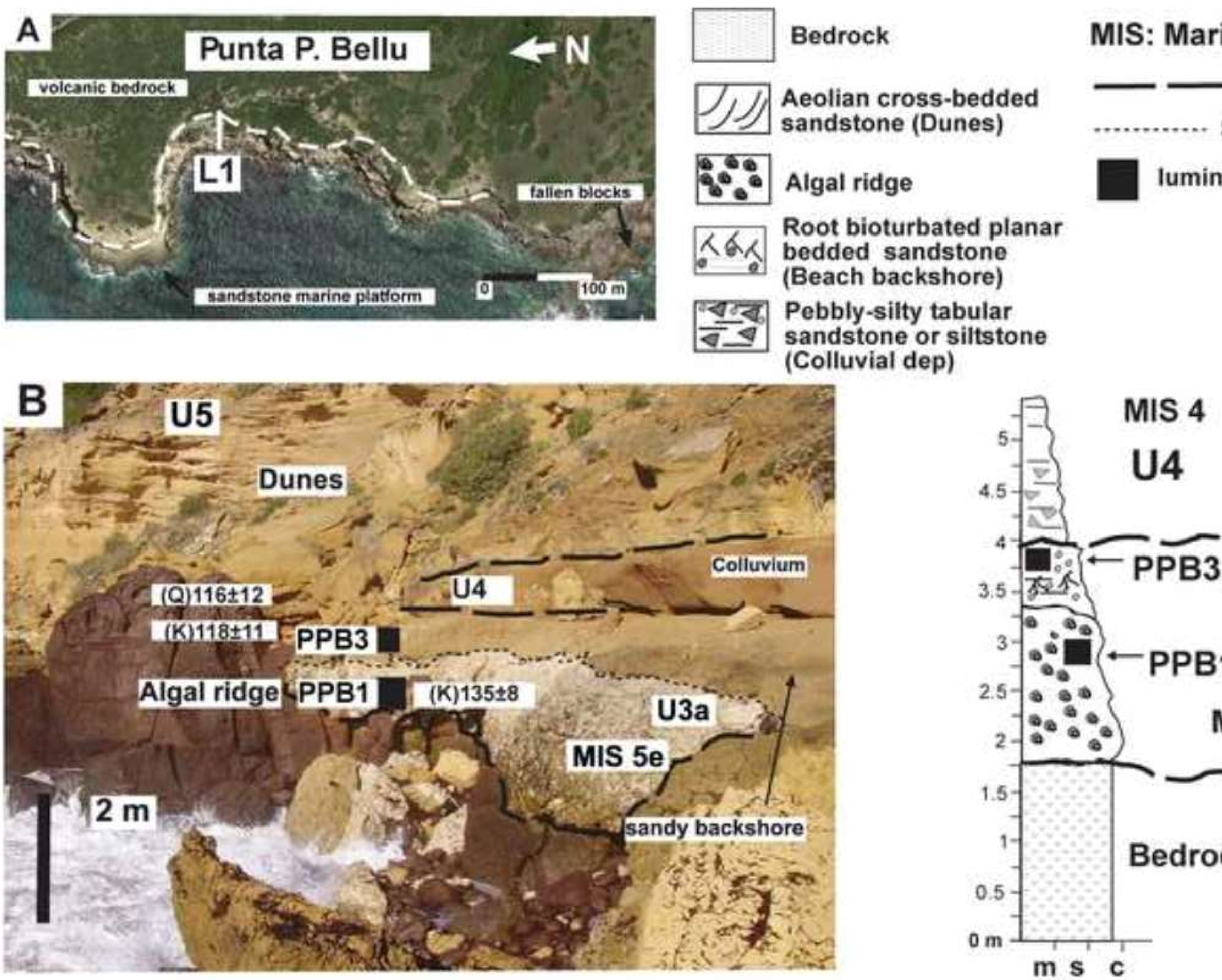

Figure

Click here to download high resolution image

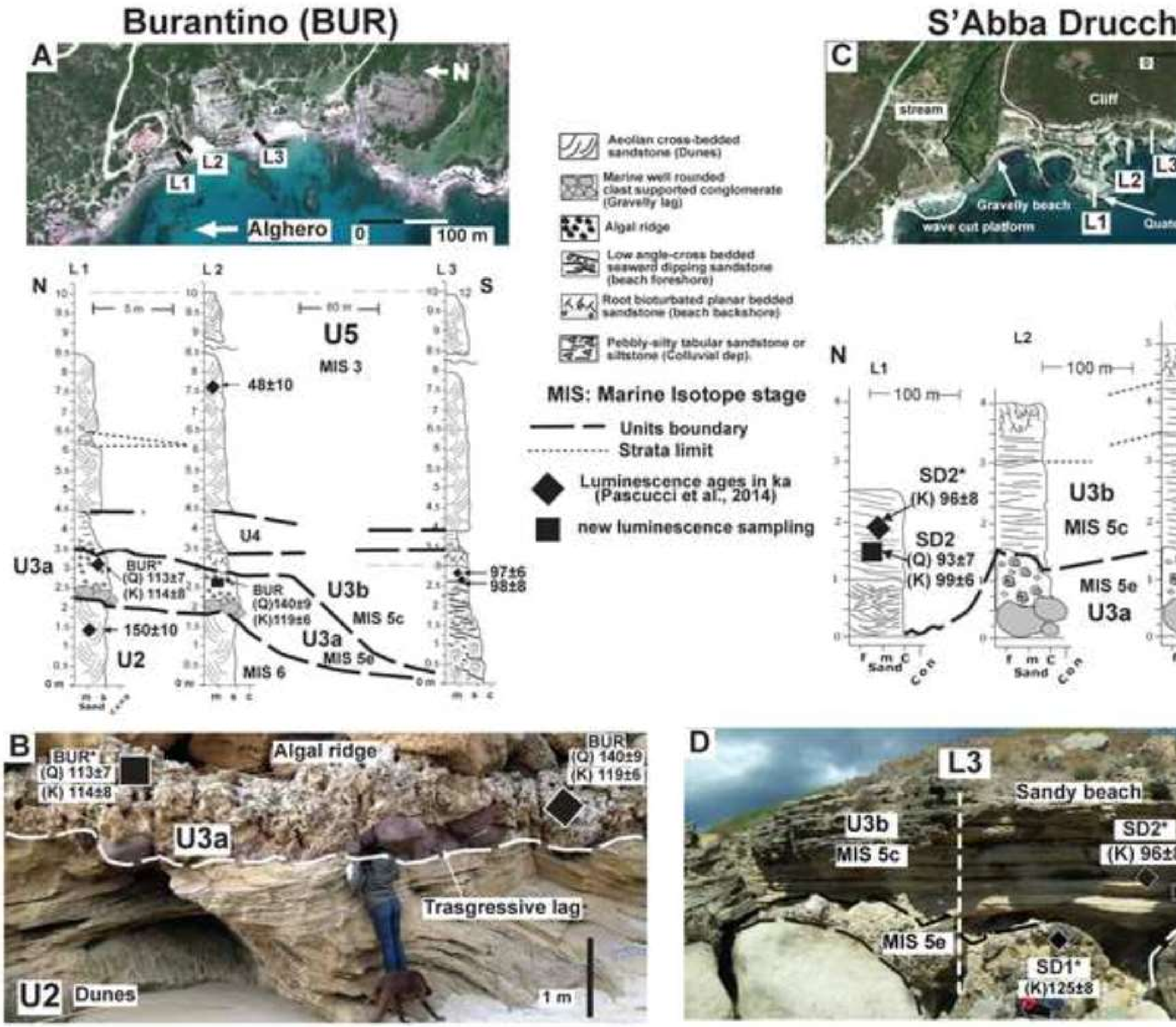

Figure

Click here to download high resolution image

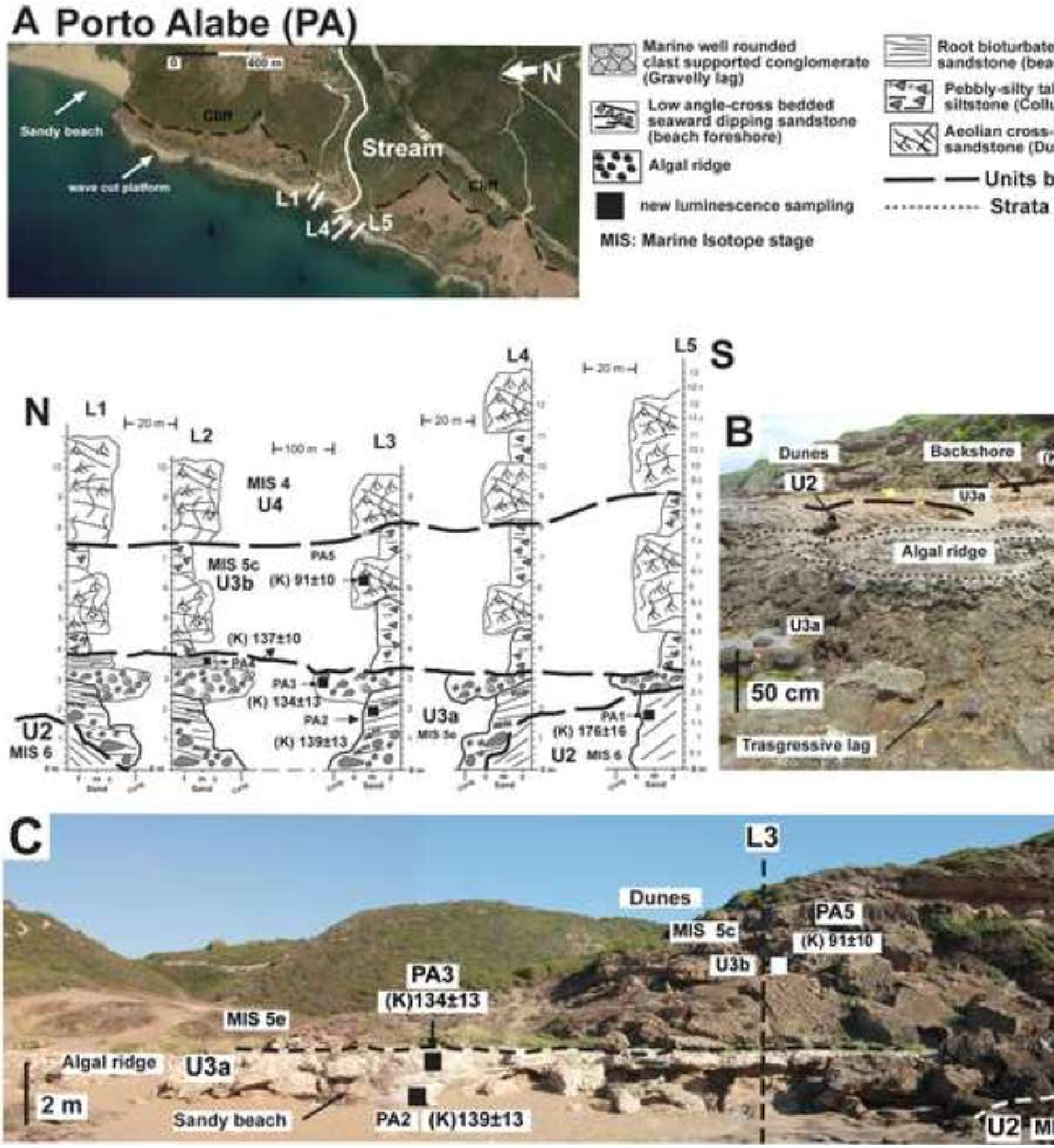

Figure
Click here to download high resolution image

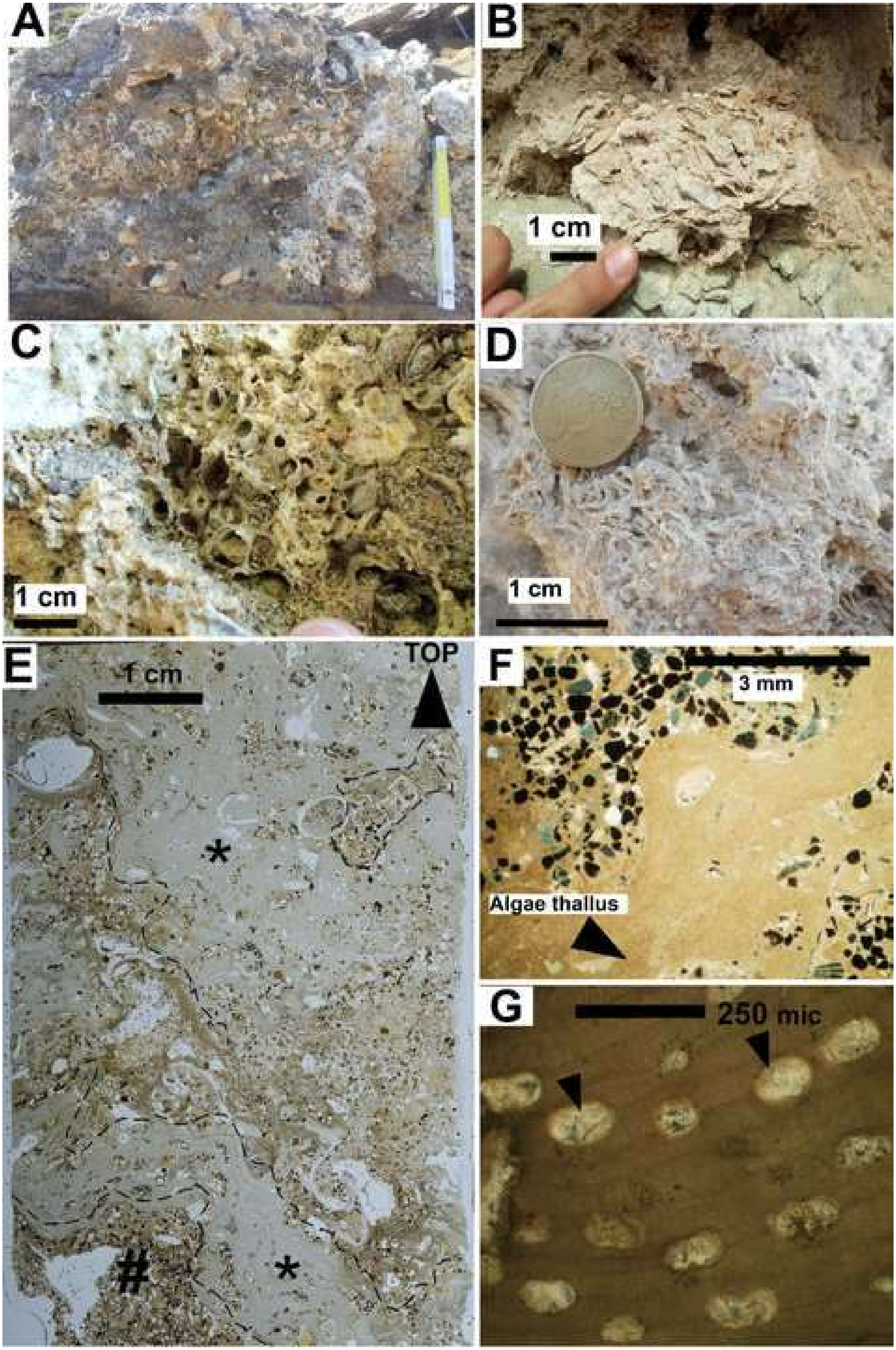

Figure
Click here to download high resolution image

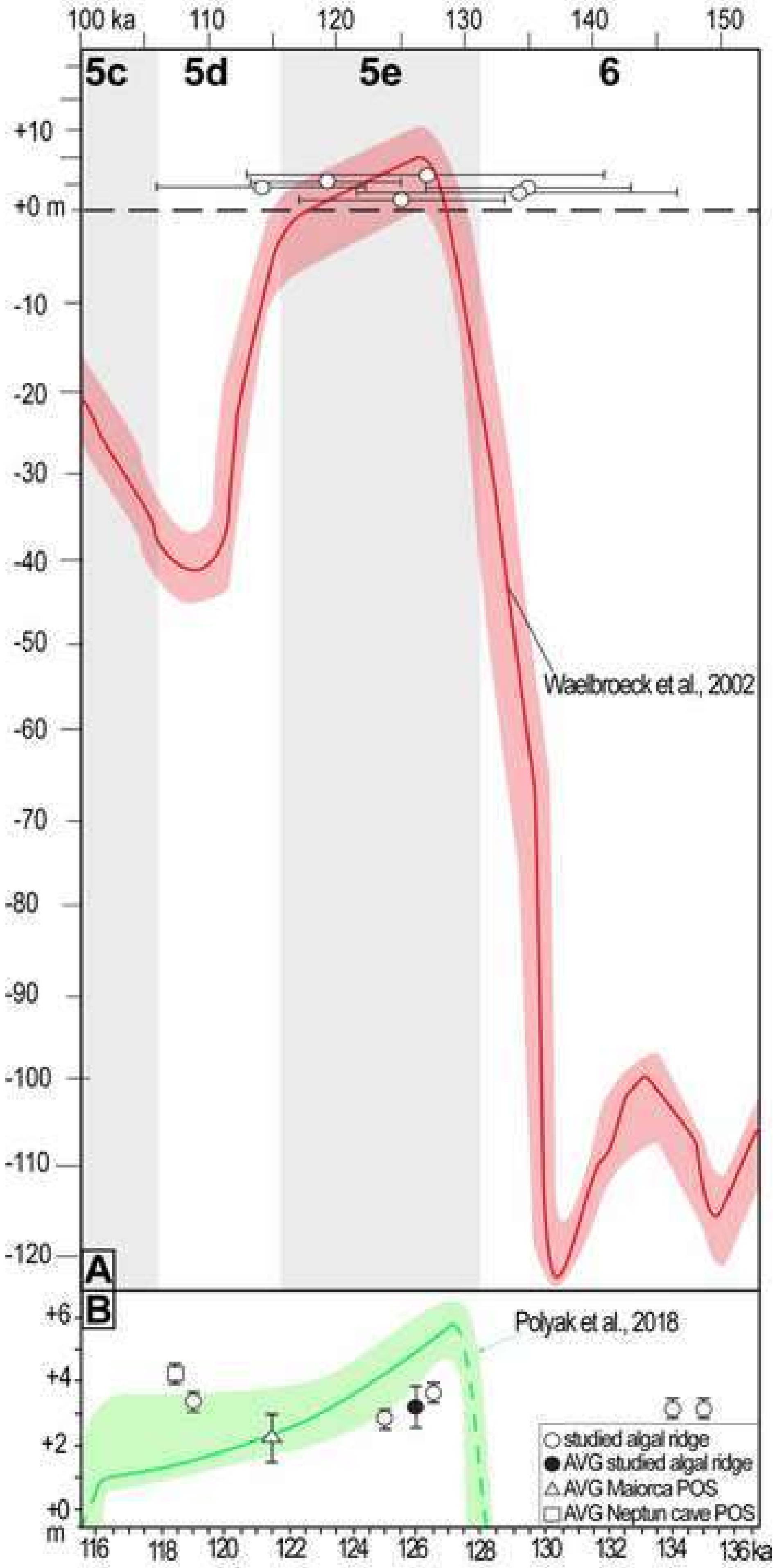

Figure
Click here to download high resolution image

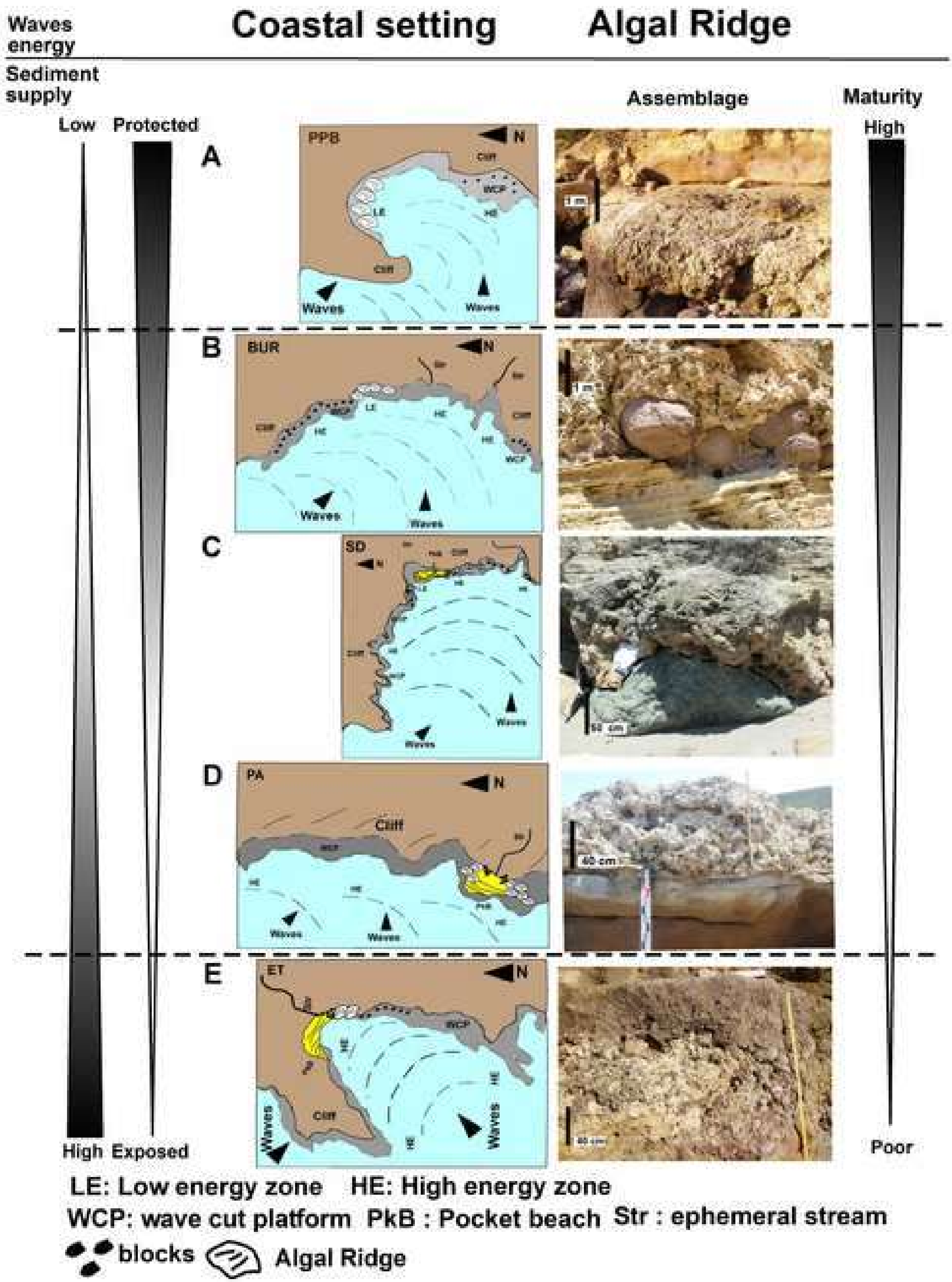

Figure

Click here to download high resolution image

Figure
Click here to download high resolution image

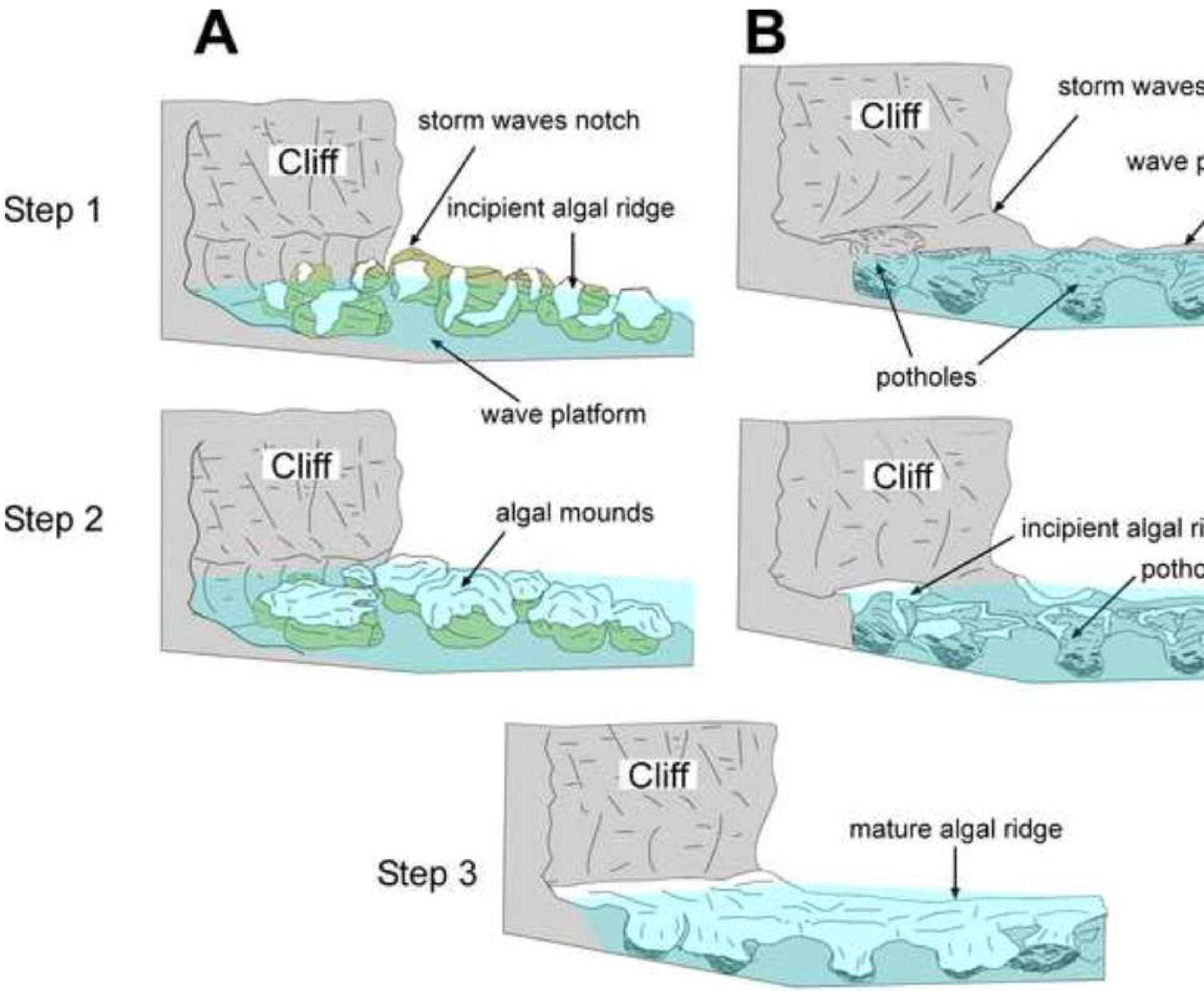

Table

Click here to download Table: Table_1_07-11-19_Rev1.docx

			Quartz OSL								
Area	**Sample**	**Facies**	**SAT (%)**	**(n)[T]**	**(n)[R]**	**OD (%)**	**Skw**	**De[W] (Gy)**	**Dr (Gy/ka)**	**SAT (%)**	**(n)**
Alghero	**CV4**	**Backshore**	37	24	20	31	-0.75	**51 ± 3**	**0.68± 0.04**	34	23
Alghero	**CV2**	**Algal Ridge**	44	34	33	29	1.87	**56 ± 4**	**0.46± 0.04**	17	26
Alghero	**PPB3**	**Backshore**	57	26	15	44	0.04	**69 ± 6**	**0.59± 0.04**	29	24
Alghero	**PPB1**	**Algal Ridge**	62	40	35	30	-0.25	**86 ± 4**	**0.42± 0.04**	36	23
Alghero	**BUR**	**Algal Ridge**	47	106	85	51	-0.28	**76± 4**	**0.54± 0.04**	38	48
Alghero	**Bur***	**Algal Ridge**	-	-	-	-	-	**95 ± 5**	**0.80± 0.04**	-	-
Bosa	**SD2***	**Beachface**	sat								
Bosa	**SD2**	**Beachface**	52	36	23	42	-0.63	**104 ± 7**	**1.12± 0.05**	45	35
Bosa	**SD1***	**Algal ridge**	sat					**-**	**-**		
Bosa	**PA5**	**Dunes (Top)**	64	35	25	38	-0.52	**149± 8**	**2.02 ± 0.07**	27	22
Bosa	**PA4**	**Backshore**	85	30	12	17	0.2	**145 ± 9**	**1.86 ± 0.07**	45	19
Bosa	**PA3**	**Algal Ridge**	30	43	13	36	-0.22	**59 ± 4**	**1.19 ± 0.05**	27	34
Bosa	**PA2**	**Beachface**	sat	18	12	17	0.01	**218 ± 14**	**1.60± 0.06**	37	30
Bosa	**PA1**	**Dunes (Base)**	74	30	18	17	0.12	**152 ± 8**	**1.46 ± 0.05**	30	35

Table

Click here to download Table: Table_2_07-11-19_Rev1.docx

Site	Facies	Age (ka)	MIS	Field Elevation (m)	Index Range (m)	Paleo Rela
El Trò	Algal Ridge	127 ± 14	MIS 5e	3.5 ± 0.1	0.3	
Punta Padre Bellu	Algal Ridge	135 ± 8	MIS 5e	3.3 ± 0.1	0.3	
Burantinu	Algal Ridge	119 ± 6	MIS 5e	3.5 ± 0.1	0.3	
Sabba Drucche	Algal Ridge	125 ± 8	MIS 5e	3.0 ±0.1	0.3	
Porto Alabe	Algal Ridge	134 ± 13	MIS 5e	3.3 ± 0.1	0.3	

***Declaration of Interest Statement**

Declaration of interests

☒ The authors declare that they have no known competing financial interests or personal relationships that could have appeared to influence the work reported in this paper.

☐The authors declare the following financial interests/personal relationships which may be considered as potential competing interests: